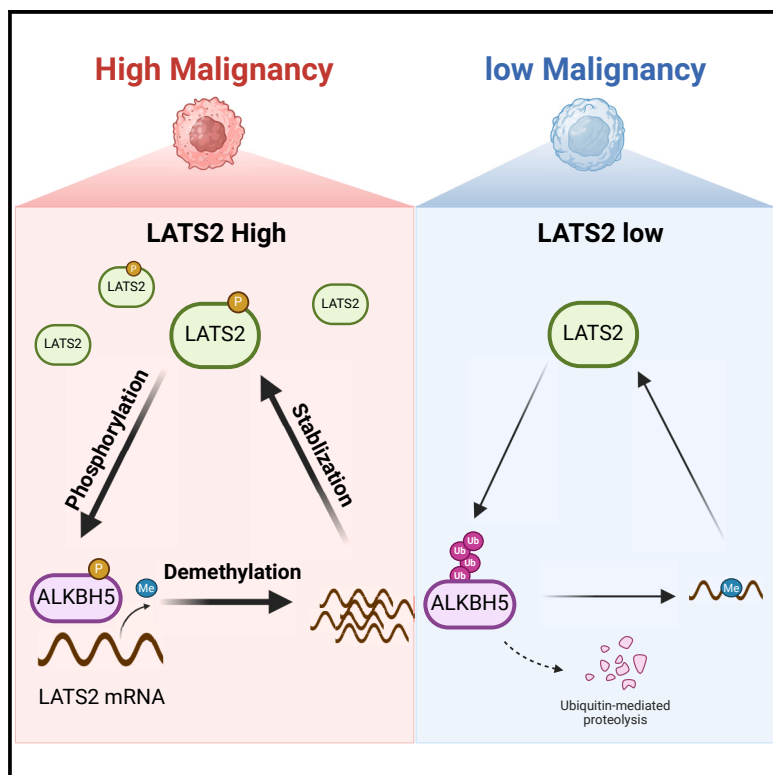


A LATS2 and ALKBH5 positive feedback loop supports their oncogenic roles

Graphical abstract



Authors

Lei Cao, Ruohui Han, Yingying Zhao, ..., Dayong Liu, Baofeng Wang, Xudong Wu

Correspondence

wuxudong@tmu.edu.cn

In brief

Cao et al. show that the MST1/2-LATS2 axis is active in glioblastoma, phosphorylates ALKBH5, and safeguards its nuclear localization and protein stability. In turn, ALKBH5 stabilizes LATS2 mRNA by demethylating m⁶A, thereby forming a positive feedback loop to promote glioblastoma progression.

Highlights

- LATS2 phosphorylates ALKBH5 at Ser361, ensuring its nuclear localization and stability
- Phosphorylated ALKBH5 in the nucleus stabilizes LATS2 mRNA by demethylating m⁶A
- The LATS2/ALKBH5 positive feedback loop is crucial for their oncogenic roles



Article

A LATS2 and ALKBH5 positive feedback loop supports their oncogenic roles

Lei Cao,¹ Ruohui Han,² Yingying Zhao,¹ Xiaoyang Qin,¹ Qian Li,¹ Hui Xiong,³ Yu Kong,¹ Ziyi Liu,¹ Zexing Li,^{1,4} Feng Dong,¹ Ting Li,¹ Xiujuan Zhao,¹ Lei Lei,¹ Qian Zhao,¹ Dayong Liu,² Baofeng Wang,⁵ and Xudong Wu^{1,6,7,*}

¹State Key Laboratory of Experimental Hematology, the Province and Ministry Co-sponsored Collaborative Innovation Center for Medical Epigenetics, Key Laboratory of Immune Microenvironment and Disease (Ministry of Education), Tianjin Key Laboratory of Medical Epigenetics, Department of Cell Biology, Tianjin Medical University, Qixiangtai Road 22, Tianjin 300070, China

²Department of Endodontics and Laboratory of Stem Cells Endocrine Immunology, Tianjin Medical University School and Hospital of Stomatology, Tianjin 300070, China

³Department of Immunology, Tianjin Medical University, Qixiangtai Road 22, Tianjin 300070, China

⁴School of Life Sciences, Tianjin University, Tianjin 300072, China

⁵Department of Neurosurgery, Tongji Hospital, Tongji Medical College, Huazhong University of Science and Technology, Wuhan 430030, China

⁶Department of Neurosurgery, Tianjin Medical University General Hospital, Tianjin 300052, China

⁷Lead contact

*Correspondence: wuxudong@tmu.edu.cn

<https://doi.org/10.1016/j.celrep.2024.114032>

SUMMARY

N(6)-methyladenosine (m^6A) critically regulates RNA dynamics in various biological processes. The m^6A demethylase ALKBH5 promotes tumorigenesis of glioblastoma, while the intricate web that orchestrates its regulation remains enigmatic. Here, we discover that cell density affects ALKBH5 subcellular localization and m^6A dynamics. Mechanistically, ALKBH5 is phosphorylated by the large tumor suppressor kinase 2 (LATS2), preventing its nuclear export and enhancing protein stability. Furthermore, phosphorylated ALKBH5 reciprocally erases m^6A from LATS2 mRNA, thereby stabilizing this transcript. Unexpectedly, LATS2 depletion suppresses glioblastoma stem cell self-renewal independent of Yes-associated protein activation. Additionally, deficiency in either LATS2 or ALKBH5 phosphorylation impedes tumor progression in mouse xenograft models. Moreover, high levels of LATS2 expression and ALKBH5 phosphorylation are associated with tumor malignancy in patients with gliomas. Collectively, our study unveils an oncogenic positive feedback loop between LATS2 and ALKBH5, revealing a non-canonical branch of the Hippo pathway for RNA processing and suggesting potential anti-cancer interventions.

INTRODUCTION

The RNA modification N(6)-methyladenosine (m^6A) holds significant importance in various biological processes. The biochemical basis for its dynamics has been made clear by intensive investigations. It is catalyzed by a methyltransferase complex mainly composed of catalytic subunit METTL3 and its interacting proteins, including METTL14, WTAP, and KIAA1429.^{1–4} Conversely, m^6A can be removed by RNA demethylases ALKBH5 (α -ketoglutarate-dependent dioxygenase alkB homolog 5)⁵ and FTO (fat mass and obesity-associated protein).⁶ A number of RNA-binding proteins, including YTHDF1/2/3, YTHDC1/2, IGF2BP1/2/3, and HNRNPs, act as m^6A readers exerting diverse effects on the fates of mRNA processing, such as facilitating RNA splicing, decay, or translation. Among them, YTHDF2 plays crucial roles in RNA decay.^{7,8}

Accumulating evidence has emerged indicating that the deregulation of m^6A dynamics plays an important role in cancer biology. Recently, numerous regulators involved in the dynamic

m^6A decoration have been shown to play roles in the generation and maintenance of cancer stem cells. One such regulator is ALKBH5, which is highly expressed in glioblastoma stem-like cells (GSCs) and predicts poor patient survival. Functional and mechanistic analyses have demonstrated that its demethylase activity is required for GSC self-renewal and tumorigenicity.^{9,10} However, the cellular contexts or signaling pathways governing the subcellular localization, abundance, and activity of ALKBH5 in GSCs remain unknown.

The highly conserved Hippo pathway plays crucial roles in controlling organ size and tissue homeostasis. Dysregulation of Hippo pathway is closely related to various human diseases, including cancers.^{11–16} The core of classical mammalian Hippo pathway is a kinase cascade leading from MST1/2 (mammalian STE20-like protein kinase 1 and 2; also known as STK4/3)/SAV1 complex to LATS1/2 (the large tumor suppressor 1 and 2)/Mob1 complex.^{17–22} This cascade ultimately phosphorylates and inhibits the activity of transcriptional coactivator YAP (Yes-associated protein)/TAZ (transcriptional coactivator with PDZ-binding



motif), thereby regulating transcriptional enhanced associate domain-mediated transcription involved in cell proliferation and survival.^{23–25} However, it remains unknown whether the Hippo pathway is linked to m⁶A dynamics.

Previous studies have convincingly established that the inactivation of the Hippo pathway or YAP/TAZ hyperactivation strikingly promotes cellular transformation and tumorigenesis in various cancer types. For examples, MST1/2 deletion or YAP overexpression in mouse liver results in tissue overgrowth and tumor development.^{24,26,27} The expression of LATS1/2, a serine/threonine protein kinase whose activation represents the major functional output of the Hippo pathway, is frequently lost in numerous types of tumors due to silencing by DNA methylation, microRNA mediated-mRNA repression or post-translational modification (PTM)-related protein degradation, but rarely through mutations.^{28–31} However surprisingly, LATS1/2 loss was recently reported to suppress the development of colorectal cancer and estrogen receptor (ER)⁺ breast cancer,^{32–34} uncovering a tumor-promoting function of LATS1/2 in certain contexts while lacking a clear molecular mechanistic insight.

Glioma is the most common type of primary brain tumor in adults.³⁵ As one of the most aggressive forms, glioblastoma (GBM, World Health Organization grade IV glioma) has been intensively studied. To date, the roles of Hippo signaling in gliomas remain poorly understood. Recently, hypermethylation of *LATS2* promoter in *IDH*-mutant low-grade glioma was reported, which is not responsible for YAP activation.³⁶ Therefore, it is necessary to clarify whether and how LATS2 plays oncogenic roles in gliomas.

Thus far, GBM has been molecularly subgrouped to proneural (PN), classical, and mesenchymal (MES) subtypes, associated with increasing degree of malignancy. Nevertheless, GBM exhibits substantial heterogeneity and contains cells that display stem-like properties at the apex.^{37–39} These GSCs are capable of self-renewal as well as differentiation into multiple lineages through stimulation, so that they are resistant to conventional therapy.⁴⁰ Understanding the molecular mechanisms for the maintenance of GSCs is critical to the development of effective therapeutic strategies.

In this study, we present evidence that LATS2 plays a positive role in promoting GBM progression. Mechanistically, we reveal that LATS2 phosphorylates ALKBH5, leading to its nuclear retention and stabilization. Interestingly, we find that the intranuclear phosphorylated form of ALKBH5 reciprocally targets LATS2 mRNA for m⁶A demethylation, thereby ensuring its stability. In addition to this *in vitro* positive feedback, we demonstrate a positive correlation between LATS2 expression levels and ALKBH5 phosphorylation in clinical glioma specimens, underscoring the clinical relevance of this regulatory interaction. Hence, our findings reveal an unanticipated interplay between LATS2 and ALKBH5, providing valuable insights into the underlying mechanisms driving malignancy progression. The elucidation of this regulatory loop holds promise in laying the foundation for potential anti-cancer therapeutic interventions aimed at targeting LATS2 and ALKBH5 and even shedding light on fresh perspectives regarding the regulation of normal development.

RESULTS

High cell confluence or serum deprivation results in m⁶A erasing by intranuclear ALKBH5

To elucidate the underlying mechanisms of m⁶A regulation by cellular metabolism, we used TPC1115 cells^{41,42} and GL261 cells, a human and a mouse GBM line, respectively, and altered cell culturing density or the ingredients of medium in culture to examine their impact on global m⁶A levels. We chose GBM cells for investigation due to substantial evidence highlighting the pivotal role of m⁶A in GBM tumorigenicity.^{9,10,43–45} In both selected GBM lines, we observed a significant reduction in m⁶A levels in cells cultured at high density (HD) compared to those at low density (LD), as evidenced by dot blot analysis. Furthermore, fetal bovine serum (FBS) deprivation in LD cells (LD-FBS) leads to a marked decrease in m⁶A levels (Figure 1A). To pinpoint the specific component of the m⁶A regulatory network affected by cell culture conditions (Figure 1B), we used specific short hairpin RNAs (shRNAs) to individually knock down the m⁶A writer METTL3, or the erasers ALKBH5 and FTO. Intriguingly, ALKBH5 KD (knockdown), but not METTL3 or FTO KD, nullifies the regulatory impact of cell culture conditions on m⁶A levels (Figures 1C–1E). Collectively, ALKBH5 contributes to m⁶A erasing under conditions of high cell confluence or FBS deprivation.

We further looked into how ALKBH5 is regulated by cell culture conditions. Intriguingly, although ALKBH5 is predominantly recognized as a nuclear protein, we observed its presence in both the cytoplasm and nucleus under LD conditions. Notably, significantly increased nuclear accumulation of ALKBH5 is evident under HD or LD-FBS conditions, as illustrated by immunofluorescence (IF) analysis (Figure 1F). In contrast, FTO remains unaffected by changes in cell density (Figure S1A). Remarkably, YAP is constitutively activated at both HD or LD cell cultures (Figure S1B), indicating a Hippo pathway-independent mechanism of YAP activation in GBM. Similar patterns of ALKBH5 subcellular localization are observed in HCT116 cells (colorectal cancer) and NIH 3T3 cells (mouse embryonic fibroblast) (Figure S1C). These findings suggest that the nuclear localization of ALKBH5 is a pivotal determinant for its m⁶A erasing function.

LATS2 phosphorylates ALKBH5 at serine 361 (S361)

PTMs of proteins play a crucial regulatory role in their subcellular localization. Because intercellular interactions and serum levels signal to the Hippo kinase cascade,^{46–48} we sought to investigate whether ALKBH5 might undergo phosphorylation. To explore this, we harvested protein lysates from TPC1115 cells overexpressing FLAG-tagged ALKBH5 and performed immunoprecipitation-mass spectrometry (IP-MS) analysis, revealing the identification of four unique phosphorylation sites. Our focus turned to S361 due to its proximity to the putative monopartite classical nuclear localization signal, consisting of amino acids 354–360 (PTHRRRG), as predicted using the NUCDISC subprogram of PSORTII⁴⁹ (Figures 2A and 2B).

Subsequently, we generated a specific antibody against phosphorylated ALKBH5 at S361 (ALKBH5S361ph). Dot blot assays confirmed that the antibody specifically recognizes the C-terminal peptides of ALKBH5 with S361 phosphorylation (Figure 2C).

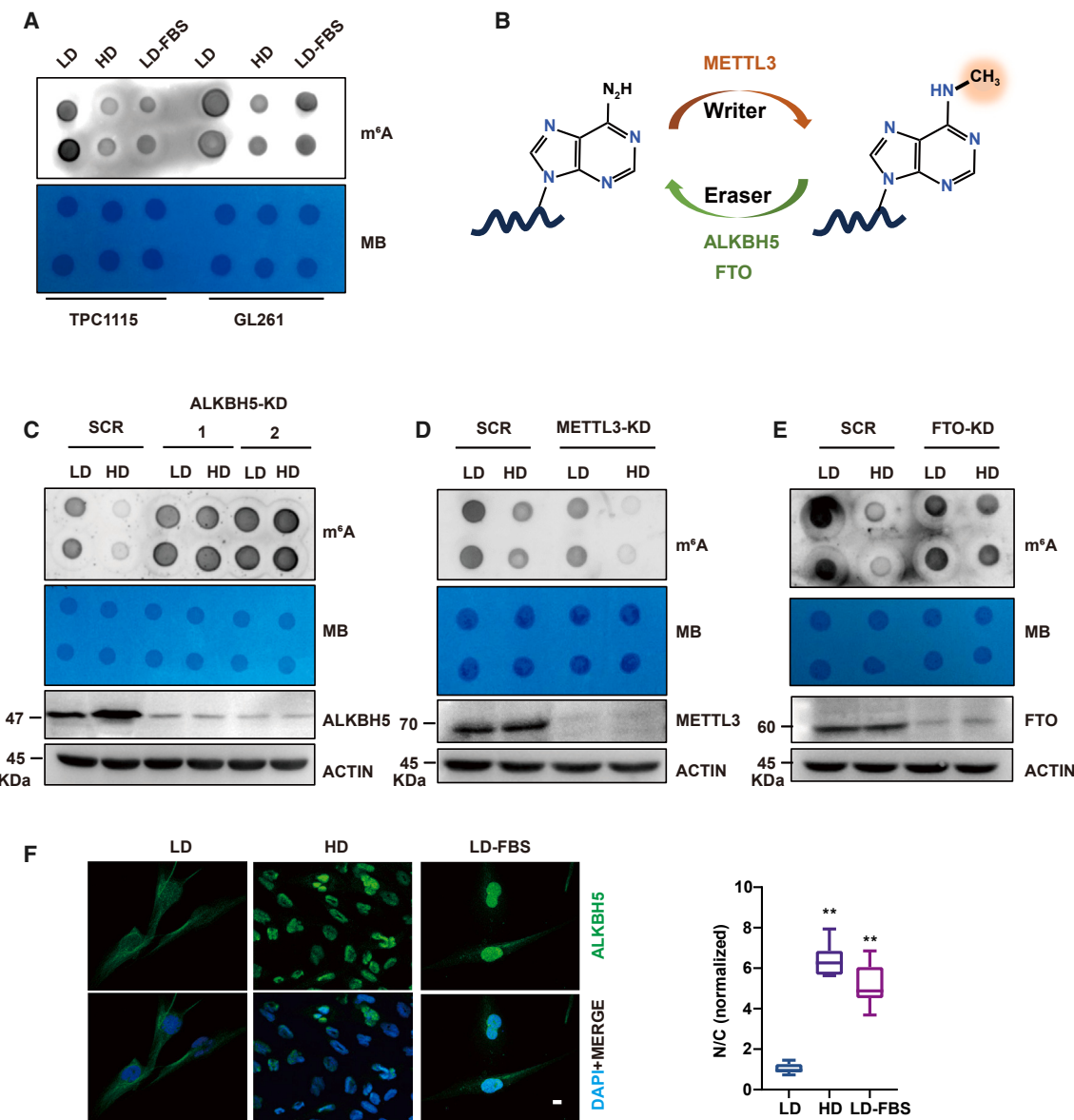


Figure 1. High cell confluence or serum deprivation results in m⁶A erasing by intranuclear ALKBH5

(A) Dot blot assays comparing m⁶A abundance in designated groups of cells under the indicated treatment. LD-FBS, low density with FBS withdrawal. Long-exp, long exposure. RNA staining with methylene blue (MB) was used as loading control.

(B) Graphical representation of m⁶A addition and demethylation.

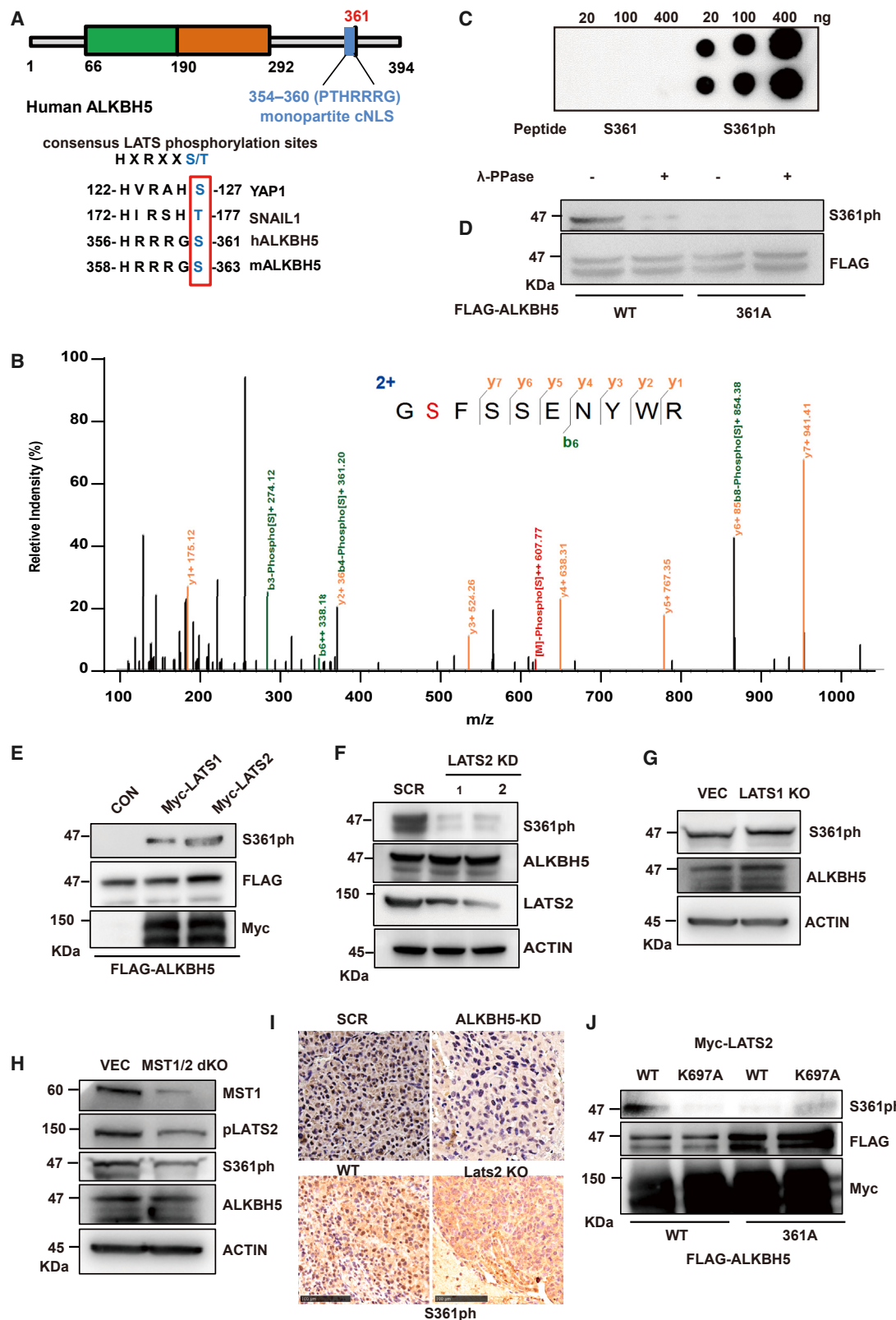
(C–E) Dot blot assays comparing m⁶A abundance in designated groups of cells under the indicated treatment with shRNA for SCR (control) as well as ALKBH5 (C), METTL3 (D), and FTO (E). RNA staining with methylene blue was used as loading control.

(F) IF analyses of ALKBH5 expression in TPC1115 cells at different culture conditions (left). The normalized nuclear to cytoplasmic (N/C) ratios of ALKBH5 signals were compared among the different culture conditions. Data are presented as mean ± SD. Significant differences are indicated: ** $p < 0.01$ (right), 2-tailed unpaired Student's t test, $n = 10$. Cells were cultured with 10% FBS cultured at different densities (LD or HD). For FBS starvation, cells were washed by PBS twice and cultured with medium without FBS for another 12 h. DAPI staining was used to identify nuclei. Scale bars, 10 μ m.

The specificity was further validated by western blot (WB) analysis of the immunoprecipitates from FLAG-tagged ALKBH5 wild-type (WT) cells and ALKBH5S361A (serine to alanine) mutant TPC1115 cells. As shown in Figure 2D, a specific band is exclusively observed in the ALKBH5 WT group, and this signal is significantly diminished following λ protein phosphatase treatment.

Thus, we have confirmed the phosphorylation of ALKBH5S361 in GBM cells.

Remarkably, the S361 residue conforms to the consensus phosphorylation motif (HXRXXS/T) of LATS (Figure 2A), a core kinase of the Hippo pathway situated directly upstream of YAP/TAZ.²⁵ Furthermore, LATS has been demonstrated to be



(legend on next page)

activated under conditions of high cell density and serum depletion.^{46–48} Accordingly, we overexpressed LATS1 and LATS2 in FLAG-ALKBH5WT expressing 293T cells. Both kinases facilitate ALKBH5S361 phosphorylation (Figure 2E).

To observe the impact of LATS1/2 deficiency on ALKBH5S361 phosphorylation, we established loss-of-function models in GBM cells. Initially, we generated *LATS1*-KO TPC1115 cells through CRISPR-Cas9 techniques, but we failed to obtain *LATS2*-deleted clones due to unknown reasons. Then, we turned to generate two LATS2-KD cell lines (LATS2 KD-1 and LATS2 KD-2) with shRNAs. WB analysis demonstrates that the depletion of LATS2, but not LATS1, results in a significant decrease in ALKBH5S361ph levels (Figures 2F and 2G). As a support, a specific activation of LATS2 by high cell confluence and serum deprivation is observed in TPC1115 and GL261 cells, whereas LATS1 signals are invisible (Figure S1D). Then, we wondered how the upstream Hippo signaling pathway affects LATS activity and ALKBH5. Through generating *MST1/2* double knockout (dKO) TPC1115 cells, we found that *MST1/2* loss significantly affects LATS2 activity and ALKBH5S361ph levels (Figure 2H). Therefore, the *MST1/2-LATS* axis is conserved in LATS2⁺ glioblastoma.

Similarly, we generated two GL261 subclones harboring homozygous frameshift mutations on *Lats2*, leading to a premature stop codon before the kinase activation domain (Figure S2A). WB and IF assays confirmed significant abrogation of LATS2 protein expression in these subclones (Figures S2B and S2C). Considering that the phosphorylation site is conserved in mouse ALKBH5 at S363 (Figure 2A), we also examined the levels of ALKBH5 phosphorylation in GL261 xenografted tumors. As shown in Figure 2I, ALKBH5 phosphorylation levels are significantly reduced in *Lats2*-null tumors, comparable to the contrast between the control and ALKBH5-KD TPC1115 xenografted tumors.¹⁰ Together, these data suggest that LATS2 plays dominant roles for ALKBH5 phosphorylation in glioblastoma cells.

To further validate this biochemical relationship, we performed *in vitro* kinase assays using immunoprecipitates from cells expressing Myc-tagged LATS2 WT or the kinase-dead form K697A mutant, with glutathione S-transferase-tagged ALKBH5 WT or S361A mutant purified from *Escherichia coli* as exogenous substrates. As shown in Figure 2J, ALKBH5 WT, but not S361A mutant, is phosphorylated by LATS2 WT, but not by K697A mutant. Hence, the kinase activity of LATS2 is indispensable for ALKBH5S361 phosphorylation.

Figure 2. LATS2 phosphorylates ALKBH5 at S361

- (A) Schematic diagram of human ALKBH5 protein. In addition to the conserved domains, S361 is shown lying in the less organized C terminus. Amino acids 354–360 (PTHRRRG) predicted by using the NUCDISC subprogram of PSORTII is presented in blue (above). Sequence alignment of the putative phosphorylated site of ALKBH5 from the indicated species (below).
- (B) Phosphopeptide of ALKBH5 was identified by MS.
- (C) Dot blot analysis of ALKBH5 phosphorylated peptide (right) and ALKBH5 non-phosphorylated peptide (left) with the ALKBH5S361ph antibody.
- (D) FLAG-tagged ALKBH5 WT or S361A mutant was immunoprecipitated and 1 set of the immunoprecipitates was treated with λ protein phosphatase as indicated. The immunoprecipitated ALKBH5 protein and phosphorylation levels were detected by WB.
- (E) ALKBH5S361ph levels were compared following overexpression of Myc-LATS1 or LATS2 in FLAG-ALKBH5-expressing 293T cells.
- (F–H) WB assays comparing ALKBH5 protein and phosphorylation levels in control and LATS2 KD WT (F), WT and *LATS1* KO cells (G), and WT and *MST1/2*dKO cells (H) TPC1115 cells, pretreated with MG132. Actin was used as loading controls.
- (I) Representative IHC staining images of ALKBH5S361ph in GBM tumor specimens from xenografts of SCR and ALKBH5-KD TPC1115 cells, WT and *Lats2*-KO GL261 cells. Scale bar, 100 μm.
- (J) *In vitro* phosphorylation of recombinant ALKBH5 (WT or S361A) protein by Myc-LATS2 (WT or K697A kinase-dead mutant). ALKBH5 S361ph and protein levels were detected by WB.

ALKBH5S361 phosphorylation is critical for its nuclear retention by shielding from nuclear exporter CRM1

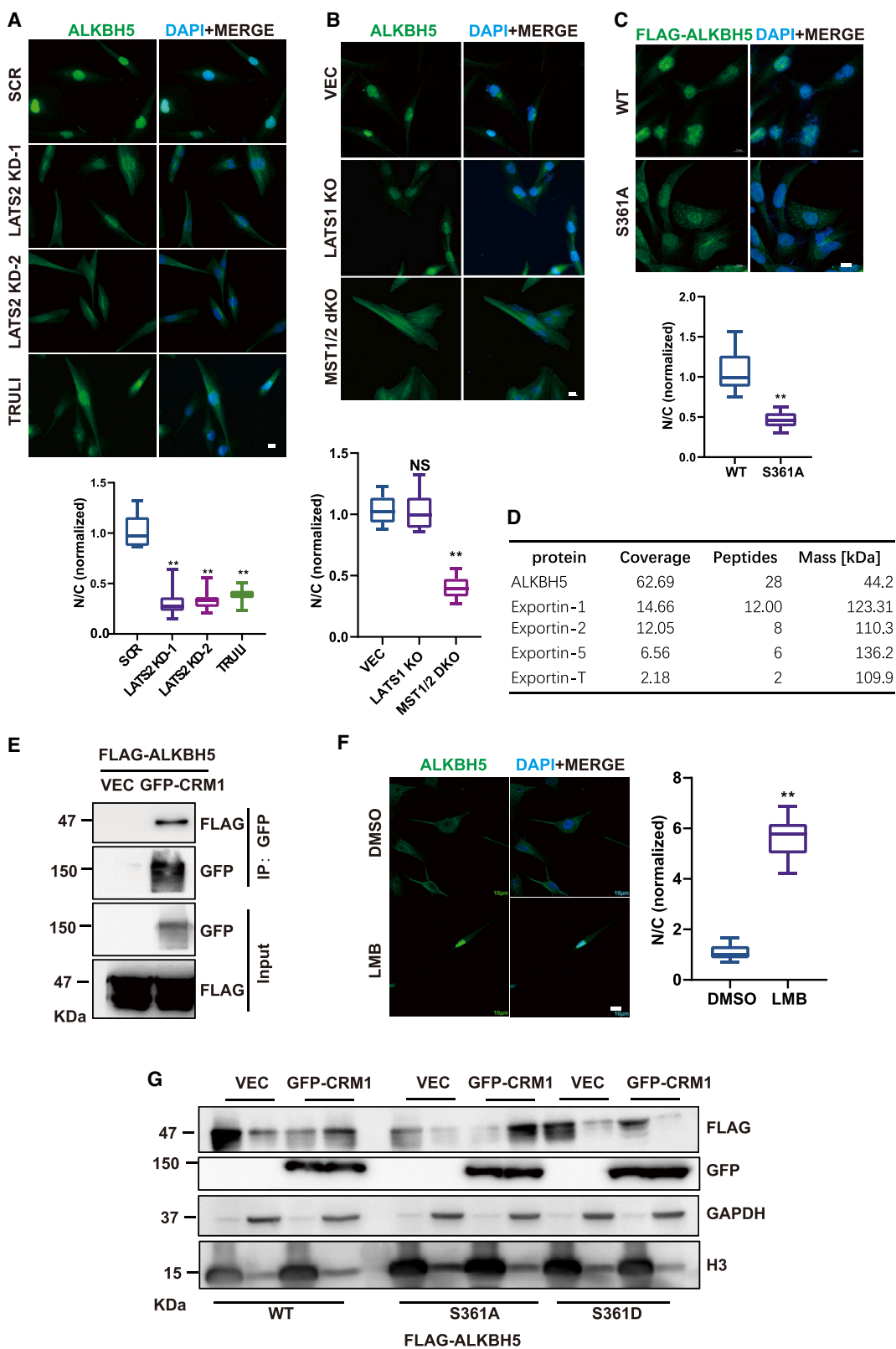
To assess whether the phosphorylation of ALKBH5 is critical for nuclear localization, we studied how LATS2 depletion or inactivation affects ALKBH5 distribution. As illustrated by IF assay, ALKBH5 signals are significantly increased in cytoplasm when LATS2 is depleted or inactivated by the LATS kinase inhibitor (Figure 3A). Consistent with the conserved MST/LATS axis, *MST1/2* loss in TPC1115 cells results in a significant shuttle of ALKBH5 to cytoplasm similar to LATS2 inactivation, whereas LATS1 deletion does not exhibit similar effects (Figure 3B). To directly link the phosphorylation of ALKBH5 to its subcellular localization, we overexpressed FLAG-tagged ALKBH5 WT or S361A in TPC1115 cells. IF analysis demonstrates that the ALKBH5S361A mutation results in a significant increase in cytoplasmic distribution (Figure 3C). Thus, these data indicate that the phosphorylation of ALKBH5 by MST/LATS2 axis favors its nuclear localization in glioblastoma.

In our previous attempt to screen potential interacting proteins of ALKBH5 by IP-MS assay (PRIDE: PXD042183),⁵⁰ we identified CRM1 (chromosome region maintenance 1, also known as exportin-1 or Xpo1) as one of the candidates (Figure 3D). Because CRM1 is a nuclear export receptor,^{51,52} we postulated that the phosphorylation of ALKBH5 may impede its nuclear export via CRM1.

We validated the interaction between ALKBH5 and CRM1 through an IP assay (Figure 3E). Subsequently, we explored whether CRM1 is responsible for ALKBH5 nuclear export, and this process is disrupted by the ALKBH5S361A mutation. When the cells cultured at LD are treated with leptomycin B (LMB), a specific CRM1 inhibitor, ALKBH5 is retained in the nucleus (Figure 3F). Conversely, upon overexpressing CRM1 in ALKBH5 WT, S361A or S361D (serine to aspartic acid, phosphomimetic mutant) TPC1115 cells, the S361A mutation facilitates ALKBH5 nuclear export by CRM1, whereas the S361D mutation confers resistance (Figure 3G). Hence, S361 phosphorylation of ALKBH5 is critical for preventing its nuclear export by CRM1, thereby ensuring its nuclear retention.

Phosphorylation of ALKBH5 S361 protects it from ubiquitin-proteasome system-dependent degradation

As shown in Figures 1C and 1G, the abundance of ALKBH5 protein appears higher in high cell density conditions. To confirm



(legend on next page)

this, we compared total levels of ALKBH5 at different cell densities. Intriguingly, ALKBH5 protein levels increase significantly with higher cell density in both TPC1115 cells and GL261 cells (Figure 4A). Remarkably, upon LATS2 depletion, the abundance of ALKBH5 protein is strikingly reduced in these two cells when cultured at comparable densities (Figure 4B). In contrast, the protein levels of other m⁶A regulators remain unaffected (Figures S3A and S3B). Moreover, RT-qPCR analysis excludes the possibility that LATS2 depletion affects ALKBH5 mRNA levels (Figure S3C). Thus, we examined whether LATS2 depletion affects ALKBH5 protein turnover. To assess this, we treated TPC1115 cells with either the proteasome inhibitor MG132 or the lysosome inhibitor BA1 and measured their effects on ALKBH5 abundance. As shown in Figure 4C, ALKBH5 protein levels increase upon MG132 treatment but not BA1 treatment, indicating that ALKBH5 stability is regulated by the ubiquitin-proteasome system.

Subsequently, we investigated whether ALKBH5 ubiquitination is influenced by cell density and, more specifically, by LATS2-mediated phosphorylation. We cultured hemagglutinin (HA)-ubiquitin (Ub)-expressing TPC1115 cells at different densities followed by a 4-h treatment with MG132. Strikingly, ALKBH5 exhibits higher levels of ubiquitination when cells are cultured at LD compared to HD (Figure 4D), suggesting that cell density affects the ubiquitination and subsequent stability of ALKBH5. Moreover, upon knock down of LATS2 and culturing cells at HD, an accumulation of ubiquitinated ALKBH5 is observed (Figure 4E). These findings indicate that LATS2 activity is crucial in preventing the polyubiquitination of ALKBH5.

To further confirm that LATS2-mediated phosphorylation of ALKBH5 at S361 prevents its ubiquitination and degradation, we compared ALKBH5 ubiquitination levels in WT and mutants. As shown in Figure 4F, the ALKBH5S361A mutant exhibits increased ubiquitination, whereas the phosphomimetic mutant S361D shows decreased ubiquitination compared to the WT. Furthermore, when we treated cells expressing ALKBH5 WT or mutants with cycloheximide (CHX), we found that the ALKBH5S361A mutant displays faster turnover, whereas S361D shows slower turnover than the WT (Figure 4G). Furthermore, the ALKBH5S361A mutation results in higher cytoplasmic staining signals under LD cell culture, which are further increased by treatment with MG132 (Figure 4H). This indicates that phosphorylation of ALKBH5 by LATS2 contributes to its nuclear retention and protects it from degradation in cytoplasm.

Figure 3. ALKBH5S361 phosphorylation is critical for its nuclear retention by shielding from nuclear exporter CRM1

(A and B) IF assays comparing ALKBH5 subcellular localization in the indicated groups of cells. (A) LATS2 inhibition by shRNA or inhibitor (TRULI). (B) LATS1 or MST1/2 knockout (KO). Cells were cultured at sparse density with medium without FBS for 12 h. The normalized N/C ratios of ALKBH5 signals were compared among the designated groups of cells. Data are presented as mean ± SD. Significant differences are indicated: ***p* < 0.01, 2-tailed unpaired Student's t test, *n* = 10, NS, non-significant.

(C) Representative IF staining of FLAG-ALKBH5 and FLAG-ALKBH5S361A (left) and statistics of N/C ratio (right). Data are presented as mean ± SD. Significant differences are indicated: ***p* < 0.01, 2-tailed unpaired Student's t test, *n* = 10.

(D) Summary of the peptides identified by MS from an FLAG purification of FLAG-ALKBH5 expressed in TPC1115 cells. Mass, observed number of peptides, and the percentage of coverage obtained by Mascot database searching (Matrix Science, UK) are indicated.

(E) WB analysis of the interaction between GFP-CRM1 and FLAG-ALKBH5.

(F) IF analysis comparing the subcellular localization of ALKBH5. Cells were cultured at sparse density and treated with 20 nM LMB for 8 h. Scale bars, 10 μm (left), and statistics of N/C ratio (right). Data are presented as mean ± SD. Significant differences are indicated: ***p* < 0.01, 2-tailed unpaired Student's t test, *n* = 10.

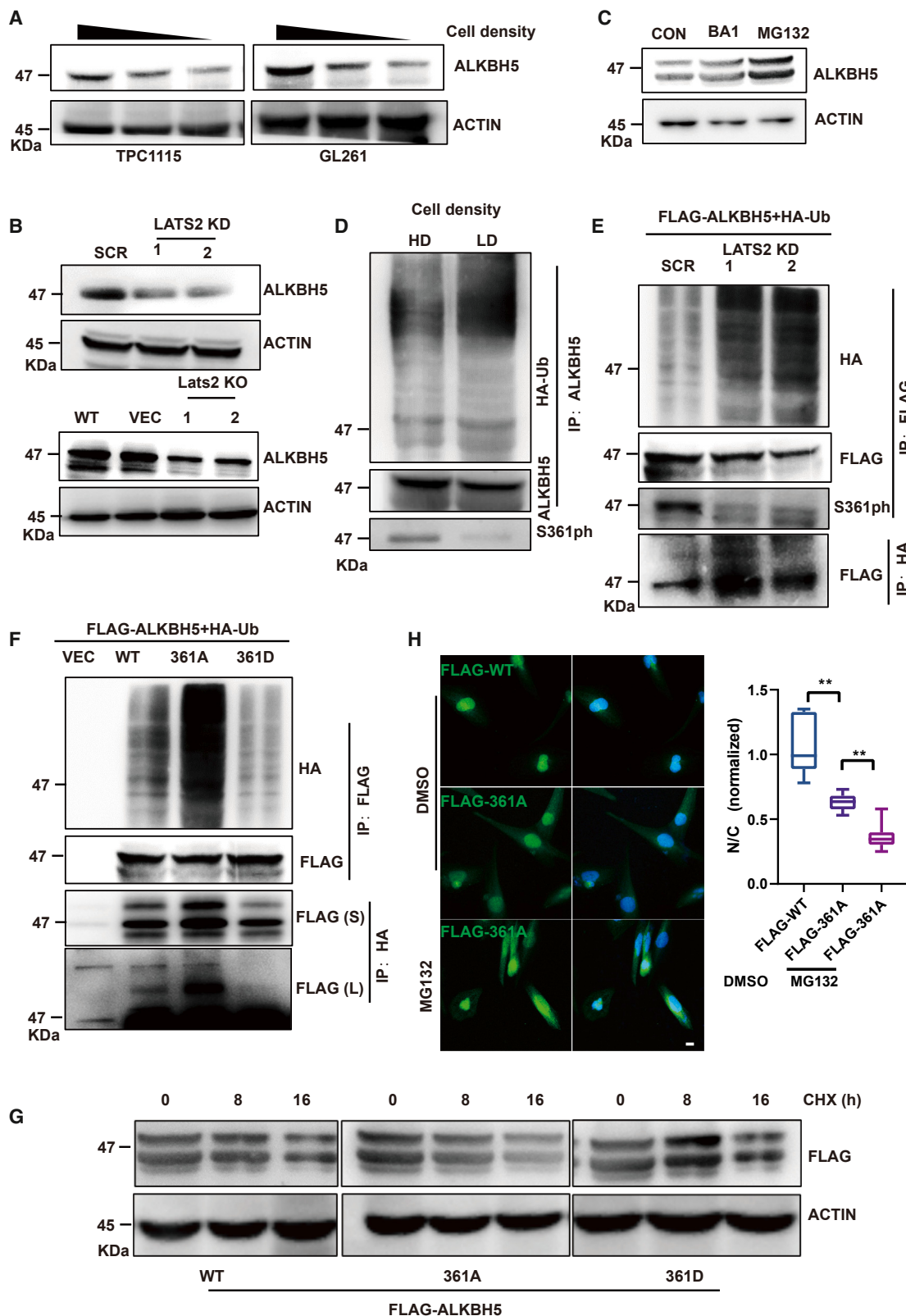
(G) WB analysis comparing the levels of FLAG-ALKBH5 and its mutants in different fractions with or without CRM1 overexpression. H3 and GAPDH (glyceraldehyde 3-phosphate dehydrogenase) serve as markers for nuclear and cytoplasm fractions, respectively.

ALKBH5S361ph is critical for m⁶A demethylation of LATS2 mRNA and its stability

Furthermore, we assessed whether the phosphorylation of ALKBH5 by LATS2 is critical for its function in m⁶A demethylation. Strikingly, loss of LATS2 leads to increased m⁶A levels (Figure 5A). Moreover, the increase in m⁶A levels caused by LATS2 loss is specifically reversed by the ectopic expression of ALKBH5-WT and S361D mutants, but not by the S361A mutant (Figure 5B). Therefore, taking a different perspective, we have linked LATS2 to the posttranscription regulatory network through its phosphorylation of ALKBH5.

Given the potential role of m⁶A demethylation in preventing RNA decay, we wondered whether LATS2 mRNA is marked with m⁶A and whether ALKBH5 erases the marks to protect mRNA stability. Through methylated RNA immunoprecipitation sequencing (MeRIP-seq) analysis in control and ALKBH5-KD TPC1115 cells, we uncovered intragenic and 3' UTRs of LATS2 mRNA marked with m⁶A, whose levels are further increased after ALKBH5 depletion. In contrast, the m⁶A signals on LATS1 are modestly decreased in ALKBH5-KD cells, excluding the possibility of regulation by ALKBH5 (Figure 5C). Among the regions, we focused on the m⁶A marks at 3' UTR due to their potential impact on LATS2 mRNA stability.⁵³ According to the MeRIP-seq data in the RMVar Database,⁵⁴ six m⁶A sites are identified within the 3' UTR of LATS2 mRNA. To assess the effects of m⁶A modifications at these sites on target gene expression, we generated luciferase reporter constructs fused with WT and mutated LATS2-3' UTR sequences (A-to-T mutations) (Figure S4A) and evaluated the luciferase activity. As shown in Figure 5D, ALKBH5 depletion reduces the luciferase activity when the reporter constructs bear the WT LATS2-3' UTR. In contrast, the A-to-T mutations within LATS2-3' UTR abolish the suppressive effects of ALKBH5 depletion on luciferase activity. In addition, RIP-qPCR analysis demonstrates a significant increase of m⁶A levels and YTHDF2 binding on LATS2 mRNA following ALKBH5 depletion, which correlates with a significant decrease in LATS2 mRNA levels (Figures 5E, 5F, and S4B). RT-qPCR analysis after actinomycin D chase assay confirms that the decrease in LATS2 mRNA levels is due to mRNA decay (Figure 5G). In the absence of YTHDF2, LATS2 mRNA levels are elevated (Figure S4C), further supporting an m⁶A-YTHDF2-dependent control of LATS2.

Moreover, the ALKBH5S361 mutant exerts a dominant-negative effect on m⁶A demethylation of LATS2, resulting in decreased



(legend on next page)

LATS2 mRNA levels (Figures 5G and 5H). Immunohistochemistry (IHC) analysis of the xenografted tumors reveals a significant decrease in LATS2 protein levels in the ALKBH5S361A group compared to the WT group (Figure 5I). Collectively, m⁶A on LATS2 mRNA is erased by the stable form of ALKBH5 within the nucleus, thereby increasing its stability.

Deficiency of LATS2 or ALKBH5S361 phosphorylation impairs GSC self-renewal and tumorigenesis

According to the above findings, stabilized LATS2 is supposed to be oncogenic, although LATS1/2 as well as other core components of the Hippo pathway have been well established as tumor suppressors. Moreover, independent studies have shown that ALKBH5 is essential for the tumorigenicity of GSC,^{9,10} which is characterized by self-renewal capability and MES properties. Hence, we initially examined the correlation between LATS2 expression levels and GSC features. In the Chinese Glioma Genome Atlas (CGGA) dataset, we observe a positive correlation between the mRNA levels of LATS2 and pluripotency markers such as SOX2 and OCT4, as well as MES markers such as FN1 and CD44. Conversely, a negative correlation is found with PN markers OLIGO1 and OLIGO2 (Figure S5A). Furthermore, using transplanting models of both mouse and human GBM cells (GL261 and TPC1115, respectively), we detect strong coexpression of LATS2 and SOX2 in tumor tissues (Figures S5B and S5C). Moreover, gene set enrichment analysis (GSEA) of RNA-seq data from the *Lats2* KO and control cells demonstrates that LATS2 loss significantly suppresses the expression of genes associated with stem cell proliferation and Hallmark epithelial-MES transition, whereas it does not affect the expression of genes in the YAP conserved signature (Figure 6A). In line with this, YAP expression or phosphorylation levels remain unaffected by *Lats2* deletion (Figure S5D). Also, LATS2 depletion leads to a substantial reduction in the expression of MES and stemness marker genes, such as CD44, FN1, and SOX2, along with an increase in the expression of differentiation marker genes, including GFAP, PDGFR, and NEFM in primary TPC1115 cells (Figure 6B). These findings suggest that LATS2 expression is crucial for sustaining the transcriptional program associated with GSC renewal independent of YAP.

We then proceeded to directly investigate the impact of LATS2 deficiency on GSC self-renewal and tumorigenesis. *In vitro* limiting dilution assays and tumor sphere formation as-

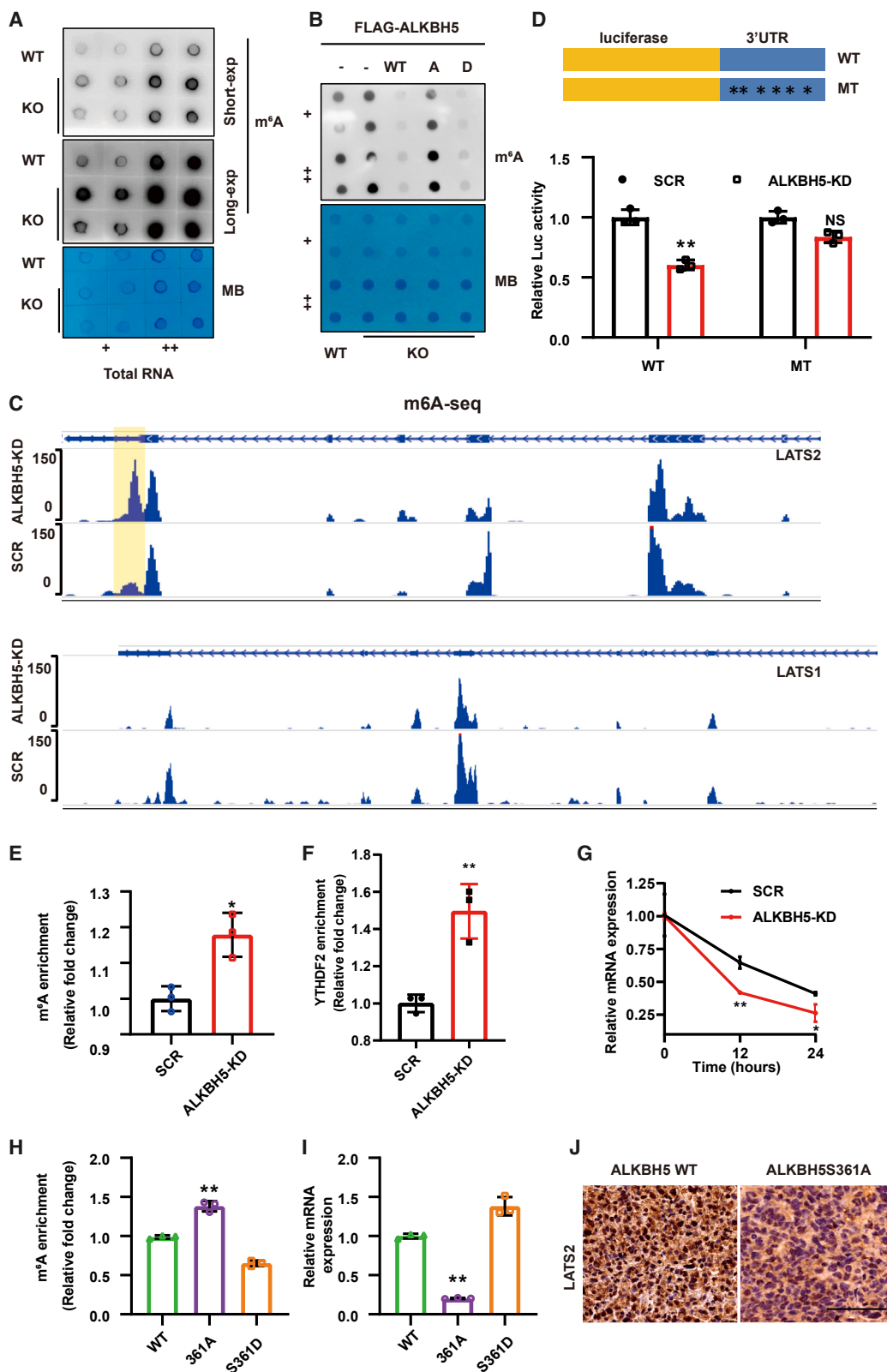
says demonstrate that LATS2 depletion leads to significant impairment of tumor sphere formation in both GL261 (Figures 6C–6E) and TPC1115 cells (Figures 6F–6H). Furthermore, we examined the effect of LATS2 depletion on GBM growth *in vivo*. Orthotopic models were established by intracerebral injection of GL261 and TPC1115 cells cotransduced with lentivirus expressing luciferase into C57BL/6J and Balb/c nude mice, respectively. Tumor growth was compared using bioluminescence imaging. In both models, LATS2 deficiency leads to a significant reduction in tumor volumes (Figures 6I and 6J) and prolonged survival of the transplanted mice (Figures 6K and 6L). Collectively, these results indicate that LATS2 is essential for GSC self-renewal and tumor progression. We further investigated the importance of ALKBH5 phosphorylation for its protumorigenic functions. Although ALKBH5S361A mutation does not affect YAP activity (Figure S5E), it significantly impairs the self-renewal capacity of TPC1115 cells *in vitro* (Figures 6M and 6N). Moreover, mice with orthotopically xenografted tumors derived from ALKBH5S361A cells exhibit significantly prolonged survival compared to those with ALKBH5WT- and S361D-expressing tumors (Figure 6O). In summary, the LATS2-ALKBH5 feedback loop plays a crucial role in the self-renewal of GSCs and the progression of tumors.

Elevated levels of LATS2 expression and ALKBH5 phosphorylation are correlated with increased tumor malignancy in glioma patients

To gain insight into the roles of Hippo signaling in glioma progression, we used the transcriptome data from The Cancer Genome Atlas and CGGA datasets of gliomas to analyze the mRNA levels of core components within the Hippo signaling pathway and their association with prognosis. Unsupervised clustering analysis demonstrates that LATS2, along with its upstream activator STK3 (MST2), MAPK14, and MAP2K3,⁵⁵ exhibits high expression levels in the high grade of gliomas (mainly grade IV; Figures 7A and S6A). The expression levels of LATS2 but not LATS1 are significantly correlated with tumor grades (Figures 7B and S6B). Furthermore, the LATS2 expression levels are significantly elevated in recurrent and secondary gliomas compared to primary gliomas. Even among the subtypes of GBM, LATS2 expression levels in MES and classical subtypes are notably higher than in the PN subtype (Figures S6C and S6D). Consistently, the low DNA methylation levels of LATS2

Figure 4. Phosphorylation of ALKBH5S361 protects it from Ub-proteasome system-dependent degradation

- (A) WB assays comparing ALKBH5 protein levels in TPC1115 cells and GL261 cells cultured at different densities. Actin was used as loading control.
- (B) WB assays comparing ALKBH5 protein levels in control and LATS2-depleted TPC1115 and GL261 cells. Actin was used as loading control.
- (C) The effects of MG132 or baflomycin A1 (BA1) treatment on the protein levels of ALKBH5. TPC1115 cells were treated with DMSO, MG132 (20 μM), or BA1 (20 nM) for 4 h before harvest for WB assay. Actin was used as loading control in WB assay.
- (D) WB analysis comparing ALKBH5 ubiquitination levels. HA-Ub-expressing TPC1115 cells cultured at LD or HD were treated with 20 mM MG132 for 4 h before harvest. Endogenous ALKBH5 was immunoprecipitated, and WB was used to detect ubiquitination and S361ph levels of ALKBH5.
- (E and F) WB analysis comparing ALKBH5 ubiquitination levels of the indicated groups of cells. (E) Cells expressing HA-Ub and FLAG-ALKBH5 were treated with SCR or LATS2 KD. (F) Cells expressing HA-Ub and FLAG-ALKBH5 as well as its mutants. Cells were treated with 20 mM MG132 for 4 h before harvest. FLAG-ALKBH5 was immunoprecipitated to detect ubiquitination and total or S361ph levels of ALKBH5. Conversely, HA-Ub was immunoprecipitated to detect FLAG-ALKBH5.
- (G) S361A mutation destabilizes ALKBH5. TPC1115 cells were transfected with indicated ALKBH5 constructs. Protein synthesis was blocked by treatment with 50 μg/mL CHX for the indicated time. Transfected ALKBH5 protein levels were detected by WB. Actin was used as loading controls in WB assays.
- (H) IF analysis comparing the subcellular localization of FLAG-tagged ALKBH5-WT or S361A TPC1115 cells (left). The normalized N/C ratios of signals were compared among the designated groups of cells. Data are presented as mean ± SD. Significant differences are indicated: **p < 0.01, 2-tailed unpaired Student's t test, n = 10 (right). To stabilize the cytoplasmic ALKBH5S361A, cells were treated with 20 mM MG132 for 4 h before IF assay.



(legend on next page)

promoter and high mRNA levels of LATS2 but not of LATS1 predict poor survival in glioma patients (Figures 7C and S6E–S6G). Hence, these findings suggest a potential association between LATS2 expression levels and malignant behavior.

Considering the deficiencies of GL261 as a GBM model, such as its high mutational load, we proceeded to examine the protein levels of LATS2 by IHC staining of resected tumor samples with varying grades of glioma (the clinical information of the specimens is listed in Table S1). As depicted in Figure 7D, a robust association is noted between LATS2 staining signal densities and tumor grades. In addition, bearing in mind that activated YAP directly induces *LATS2* transcription to form a negative feedback loop in tumors,⁵⁶ we compared the signals of LATS2 and YAP. Through IF staining of tumor tissues xenografted with mouse glioblastoma cells GL261, we found that only a limited number of LATS2⁺ cells exhibit nuclear YAP, indicating that YAP activation is not a primary cause of LATS2 expression in GBM (Figure S6H). Collectively, high expression levels of LATS2 serve as a reliable indicator of glioma malignancy, irrespective of YAP involvement.

Having demonstrated that LATS2 and ALKBH5 exert positive regulatory functions on each other in experimental systems, we proceeded to evaluate the clinical relevance of the LATS2–ALKBH5 loop. Analysis of the CGGA datasets reveals a positive correlation between the mRNA levels of LATS2 and ALKBH5 in all grades of gliomas (Pearson correlation coefficient $R = 0.44$, $p = 4.28e-12$), whereas the mRNA levels of LATS1 and ALKBH5 exhibit a negative correlation (Figure 7E). To further validate these findings, we examined the protein levels of LATS2 and ALKBH5S361ph in human glioma specimens by IHC. Quantification of staining demonstrates a significant positive correlation between the LATS2 expression levels and ALKBH5S361ph levels ($R = 0.57$, $p = 1.4e-9$) (Figures 7F and 7G). Hence, these compelling results provide additional support for the existence of a positive feedback loop between LATS2 and ALKBH5 in the context of human malignancy.

DISCUSSION

Dynamics of m⁶A have been extensively observed during cell differentiation and development.⁵⁷ In addition, the regulation of m⁶A modification in rapid response to various stress conditions has attracted a huge amount of attention.^{10,58–61} However, the signaling pathways responsible for stress-induced m⁶A alterna-

tions and how cellular stress modulates m⁶A-modifying proteins remain elusive.

The interplay of the Hippo pathway with other signaling pathways plays a pivotal role in responding to diverse stress stimuli originating from, for example, hypoxia, reactive oxygen species (ROS), and mechanical forces. As one of the m⁶A demethylases, ALKBH5 expression has been found to be induced by hypoxic stress.^{10,62} Under conditions of ROS accumulation, ALKBH5 SUMOylation levels increase,⁶⁰ which may explain the presence of two bands of ALKBH5 in our WB assays. Functional studies of ALKBH5 have primarily been conducted under optimized cell culture conditions, often overlooking the potential influence of ALKBH5 in subcellular localization. In this study, we took gliomas as the primary models and unveiled a hitherto undiscovered regulatory dimension in the functional repertoire of ALKBH5. Specifically, high cell density or stresses such as serum deprivation enhance LATS2 activity for ALKBH5 phosphorylation, thereby preventing its nuclear export by CRM1 and safeguarding it from degradation in cytoplasm. In turn, ALKBH5 demethylates m⁶A on LATS2 mRNA, leading to the stabilization of its expression. This establishes a positive feedback loop, as long as LATS2 is not transcriptionally silenced or mutated (Figure 7H), thereby contributing to its oncogenic roles. Considering that ALKBH5 exhibits protumorigenic functions in various cancers,^{9,63–65} our finding of LATS2-mediated ALKBH5 phosphorylation expands horizons in understanding how tumor cells adapt to stressful environments.

Given the well-established protumorigenic functions of YAP activation, it becomes evident that the oncogenic roles of LATS1/2 cannot be attributed to their negative regulation of YAP activity. In fact, both of our dataset analyses and transcriptome profilings in LATS2-null glioma models have distinguished the role of LATS2 from the canonical Hippo pathway (Figures 6A, 7A, and S6). Although we do not completely understand how LATS2 localizes within the nucleus, we have clearly identified ALKBH5 as a key hub for LATS2 and unveiled a potential non-canonical Hippo pathway.

It is worth noting that most of the current studies supporting the oncogenic functions of LATS have relied on double deletion of *LATS1* and *LATS2*.^{32–34} However, according to our dataset and WB analyses, LATS1 and LATS2 exhibit differential expression patterns in gliomas, and specifically, LATS2 expression in glioma predicts an unfavorable prognosis. Moreover, our study highlights LATS2 as a crucial substrate of ALKBH5, providing

Figure 5. ALKBH5S361ph is critical for m⁶A demethylation of LATS2 mRNA and its stability

(A and B) Dot blot assays comparing m⁶A abundance in designated groups of cells under the indicated treatment. Specifically, total RNAs were used to detect m⁶A level in WT and Lats2 KO cells (A) as well as cells co-expressing FLAG-ALKBH5 or its mutants (B). Long-exp, long exposure; Short exp, short exposure; +, 100 ng; ++, 400 ng. RNA staining with methylene blue (MB) was used as loading control.

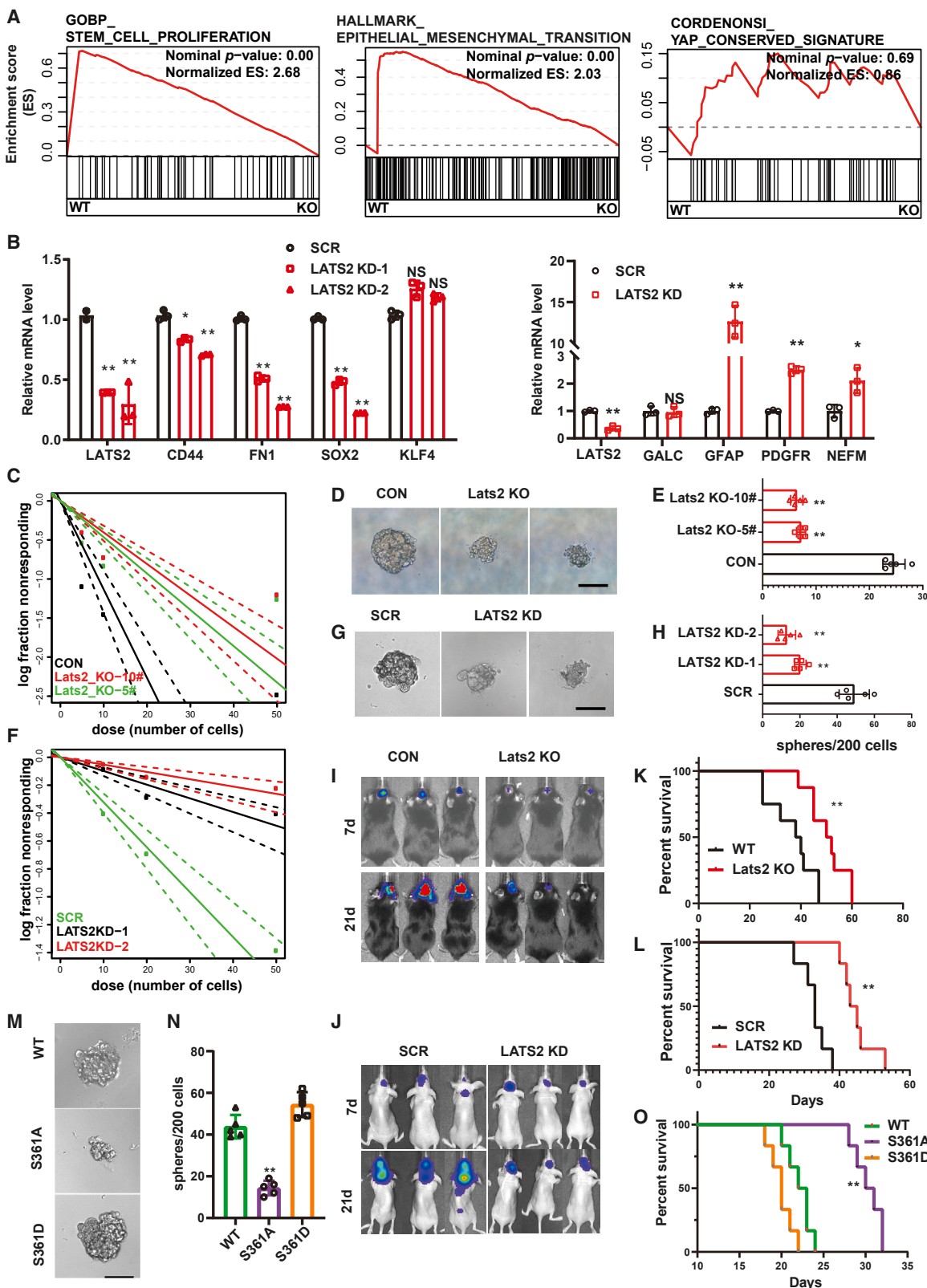
(C) Genome browser of m⁶A peaks on LATS1 and LATS2 mRNAs in control and ALKBH5-KD cells.

(D) Relative luciferase activity of LATS2-3' UTR with either WT or mutant (A-to-T mutation) m⁶A sites in control or ALKBH5 KD HEK293T cells. Firefly luciferase activity was measured and normalized to Renilla luciferase activity. Data are presented as mean ± SD. Significant differences are indicated: ** $p < 0.01$, 2-tailed unpaired Student's t test, $n = 3$.

(E, F, and H) m⁶A or YTHDF2 RIP-qPCR analysis comparing m⁶A levels or YTHDF2 recognition on LATS2-3' UTR in the indicated groups of TPC1115 cells. Data are presented as mean ± SD. Significant differences are indicated: ** $p < 0.01$, 2-tailed unpaired Student's t test, $n = 3$.

(G and I) RT-qPCR analysis comparing the mRNA levels of LATS2 in indicated groups of TPC1115 cells. Specifically, actinomycin D chase experiments were used to determine mRNA half-lives in control or ALKBH5 KD TPC1115 cells in (G) and the mRNA levels of LATS2 were detected in groups overexpressing ALKBH5 or its mutant (I). Two-tailed unpaired Student's t test for (E)–(I). Data are presented as mean ± SD. Significant differences are indicated: * $p < 0.05$, ** $p < 0.01$, 2-tailed unpaired Student's t test, $n = 3$.

(J) IHC analyses comparing LATS2 levels in xenografted tumors with ALKBH5-WT or S361A TPC1115 cells.



(legend on next page)

fresh perspectives on how LATS2 maintains high expression levels at least in certain cancer types. Whereas LATS2 has demonstrated oncogenic roles in our systems, the potential tumor suppressive roles of LATS1 remain to be explored. In addition, it is noteworthy that targeting both LATS1 and LATS2 in cancers may lead to uncontrollable YAP/TAZ hyperactivation, making it technically challenging for clinical application. Therefore, a more comprehensive investigation into the functional disparities between LATS1 and LATS2 is necessary to gain a deeper understanding of their roles beyond the Hippo pathway. Based on existing evidence, we believe that selective inhibition of LATS2 may represent an optimized therapeutic strategy for certain cancer types such as gliomas.

Nevertheless, the overall augmentation in m⁶A demethylation, as observed in LATS2-active cells (Figures 1 and 5) is likely to yield diverse effects across a wide array of downstream effectors. These effects may vary depending on the specific m⁶A readers involved.^{7,8} Consequently, the role of LATS2 may manifest as either an oncogene or a tumor suppressor in different contexts. In LATS2-high cancers, ALKBH5 may positively regulate other protumorigenic factors such as FOXM1.⁹ In contrast, from the perspective of organ size control, the LATS2-ALKBH5S361ph axis may also activate the expression of tumor suppressor genes. As a result, the inactivation of LATS2, in conjunction with deletion or transcriptional silencing induced by DNA hypermethylation of relevant tumor suppressor genes, may precipitate malignant transformation. Hence, our findings are expected to stimulate substantial interest in further investigating the multifaceted effects of the Hippo pathway on m⁶A regulation in both physiological and pathophysiological contexts.

In summary, our study has elucidated the engagement of LATS2 in a feedback loop with ALKBH5, serving as a key hub that transmits signals to a wide range of substrates for posttranscriptional regulation. This discovery unveils a non-canonical Hippo signaling pathway, paving the way for future investigations in developmental biology, cancer biology, and beyond.

Limitations of the study

This study establishes an unexpected LATS2/ALKBH5 positive feedback loop underlying their oncogenic roles in gli-

blastoma. Although our data strongly indicate that phosphorylation of ALKBH5 at S361 impedes CRM-mediated nuclear export, as recently reported,⁶⁶ the specific E3 ubiquitin ligase responsible for ALKBH5 ubiquitination in cytoplasm remains to be identified. Regarding LATS2, it is regulated by MST1/2, the conserved upstream Hippo pathway; however, it does not seem to control downstream YAP activity in glioblastoma. Further studies are required to find out which factors are responsible for the stable nuclear localization of YAP in glioblastoma. Due to the limitations of cell models, it cannot be ruled out that LATS1 exhibits similar regulatory functions in other systems. Notably, our findings are based mainly on widely used GBM cell models. Further validation in patient-derived cell lines and clinical GBM specimens is imperative to strengthen our conclusions.

STAR★METHODS

Detailed methods are provided in the online version of this paper and include the following:

- **KEY RESOURCES TABLE**
- **RESOURCE AVAILABILITY**
 - Lead contact
 - Materials availability
 - Data and code availability
- **EXPERIMENTAL MODEL AND STUDY PARTICIPANT DETAILS**
 - Cell culture
 - Animal model
 - Human tumor samples and ethics approval
- **METHOD DETAILS**
 - Plasmid construction
 - Co-IP, western blot, and luciferase reporter assays
 - Dot blot
 - Intracranial Xenotransplantation
 - IHC and IF
 - RT-qPCR and MeRIP-qPCR analysis
 - RNA-seq, MeRIP-seq and data analysis
- **QUANTIFICATION AND STATISTICAL ANALYSIS**

Figure 6. Deficiency of LATS2 or ALKBH5S361 phosphorylation impairs GSC self-renewal and tumorigenesis

- (A) GSEA analyses of the RNA-seq data of GL261 WT and LATS2 KO cells.
- (B) RT-qPCR analysis of the mRNA expression level of genes associated with GSC features. Data are presented as mean ± SD. Significant differences are indicated: *p < 0.05, **p < 0.01, 2-tailed unpaired Student's t test, n = 3.
- (C and F) *In vitro* limiting dilution assays for control or LATS2-depleted GL261 cells (C) or TPC1115 cells (F). After plating decreasing number of cells, frequency and probability estimates of sphere formation were computed using ELDA software.
- (D and G) Representative images of tumor spheres in dose of 5 cells/well of GL261 (D) and TPC1115 (G) cells are shown.
- (E and H) Control or LATS2-depleted GL261 cells (E) or TPC1115 cells (H) (200 cells/well) were cultured for 2 weeks, and total sphere numbers in the wells were recorded at each group. Data are presented as mean ± SD. Significant differences are indicated: *p < 0.05, **p < 0.01, 2-tailed unpaired Student's t test, n = 5.
- (I and J) Luciferase-expressing control or LATS2-depleted GL261 or TPC1115 cells (2 × 10⁵ each) were intracranially implanted into C57BL/6J mice (I) or nude mice (J), respectively. Representative luciferase images of 3 mice per group are shown over time after tumor implantation. Color scale for GL261, minimum = 1.00e-6; maximum = 5.00e-7. Color scale for TPC1115, minimum = 8.83e-4; maximum = 8.68e-6.
- (K and L) Survival analysis of mice intracranially implanted with designated groups of GL261 cells (K) or TPC1115 cells (L). Significance was determined using log rank analysis. **p < 0.01; n > 5 for each group.
- (M) Representative images of tumor spheres in dose of 5 cells/well of ALKBH5-depleted TPC1115-expressing ALKBH5-WT and its mutants.
- (N) Sphere formation rate of the indicated groups is shown. Data are presented as mean ± SD. Significant differences are indicated: *p < 0.05, **p < 0.01, 2-tailed unpaired Student's t test, n = 5.
- (O) Survival analysis of mice intracranially implanted with designated TPC1115 cells. Significance was determined using log rank analysis. **p < 0.01; n > 5 for each treatment group.

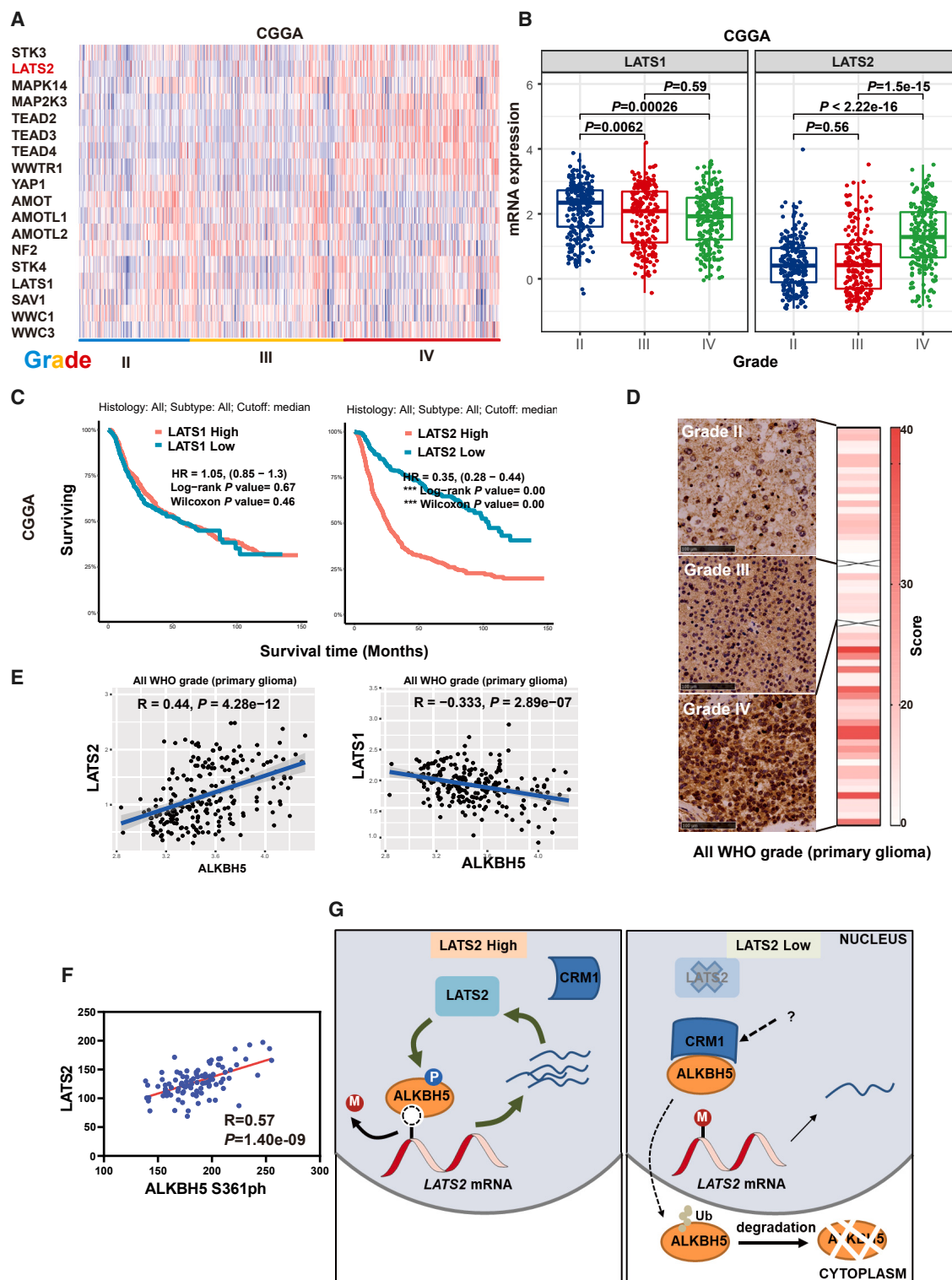


Figure 7. Positive correlation between ALKBH5 phosphorylation and LATS2 expression levels in clinical glioma specimens

(A) Heatmap comparing the mRNA levels of core components of the Hippo pathway, classified by tumor grades of glioma patients in the CGGA databases.

(B) Bar plots comparing the mRNA levels of LATS1 and LATS2 in the CGGA databases.

(C) Kaplan-Meier survival curves of glioma patients with high or low levels of LATS1/2, according to the CGGA databases.

(D) Representative IHC staining images and quantitative analysis of LATS2 protein levels in human glioma specimens. Scale bar, 100 μ m.

(legend continued on next page)

SUPPLEMENTAL INFORMATION

Supplemental information can be found online at <https://doi.org/10.1016/j.celrep.2024.114032>.

ACKNOWLEDGMENTS

This work was supported by the National Natural Science Foundation of China (32320103009, 31970579, 82103247, and 31701126), the National Key Research and Development Project of Stem Cell and Transformation Research (2019YFA0112100), the Key Research Project of Tianjin Education Commission (2020ZD13), the national youth talent support program, Tianjin Medical University Talent Excellence Program, and Tianjin Postgraduate Research Innovation Project (2021YJSB273, 2021YJSB274). We thank the Core Facility of Research Center of Basic Medical Sciences, high performance computing (HPC) platform at Tianjin Medical University for technical support. We also thank Professors Ping Wang (Tongji University) and Shian Wu (Nankai University) for providing plasmids for CRM1 overexpression and LATS2 KD, respectively.

AUTHOR CONTRIBUTIONS

L.C. and X.W. conceived of and designed the study. L.C., R.H., H.X., Z. Liu, F.D., T.L., X.Z., L.L. and Z. Li performed the cellular experiments. L.C., Y.Z., and Y.K. performed the *in vivo* experiments. L.C., X.W., Q.L., and Q.Z. created the bioinformatics analyses. L.C. and X.W. wrote the manuscript. D.L. and B.W. helped to revise the draft.

DECLARATION OF INTERESTS

The authors declare no competing interests.

Received: November 22, 2023

Revised: February 9, 2024

Accepted: March 18, 2024

Published: April 2, 2024

REFERENCES

1. Liu, J., Yue, Y., Han, D., Wang, X., Fu, Y., Zhang, L., Jia, G., Yu, M., Lu, Z., Deng, X., et al. (2014). A METTL3-METTL14 complex mediates mammalian nuclear RNA N6-adenosine methylation. *Nat. Chem. Biol.* 10, 93–95. <https://doi.org/10.1038/nchembio.1432>.
2. Wang, Y., Li, Y., Toth, J.I., Petroski, M.D., Zhang, Z., and Zhao, J.C. (2014). N6-methyladenosine modification destabilizes developmental regulators in embryonic stem cells. *Nat. Cell Biol.* 16, 191–198. <https://doi.org/10.1038/ncb2902>.
3. Ping, X.L., Sun, B.F., Wang, L., Xiao, W., Yang, X., Wang, W.J., Adhikari, S., Shi, Y., Lv, Y., Chen, Y.S., et al. (2014). Mammalian WTAP is a regulatory subunit of the RNA N6-methyladenosine methyltransferase. *Cell Res.* 24, 177–189. <https://doi.org/10.1038/cr.2014.3>.
4. Schwartz, S., Mumbach, M.R., Jovanovic, M., Wang, T., Maciag, K., Bushkin, G.G., Mertins, P., Ter-Ovanesyan, D., Habit, N., Cacchiarelli, D., et al. (2014). Perturbation of m6A writers reveals two distinct classes of mRNA methylation at internal and 5' sites. *Cell Rep.* 8, 284–296. <https://doi.org/10.1016/j.celrep.2014.05.048>.
5. Zheng, G., Dahl, J.A., Niu, Y., Fedorcsak, P., Huang, C.M., Li, C.J., Vågbø, C.B., Shi, Y., Wang, W.L., Song, S.H., et al. (2013). ALKBH5 is a mammalian RNA demethylase that impacts RNA metabolism and mouse fertility. *Mol. Cell* 49, 18–29. <https://doi.org/10.1016/j.molcel.2012.10.015>.
6. Jia, G., Fu, Y., Zhao, X., Dai, Q., Zheng, G., Yang, Y., Yi, C., Lindahl, T., Pan, T., Yang, Y.G., and He, C. (2011). N6-methyladenosine in nuclear RNA is a major substrate of the obesity-associated FTO. *Nat. Chem. Biol.* 7, 885–887. <https://doi.org/10.1038/nchembio.687>.
7. Fu, Y., Dominissini, D., Rechavi, G., and He, C. (2014). Gene expression regulation mediated through reversible m(6)A RNA methylation. *Nat. Rev. Genet.* 15, 293–306. <https://doi.org/10.1038/nrg3724>.
8. Wang, X., and He, C. (2014). Reading RNA methylation codes through methyl-specific binding proteins. *RNA Biol.* 11, 669–672. <https://doi.org/10.4161/rna.28829>.
9. Zhang, S., Zhao, B.S., Zhou, A., Lin, K., Zheng, S., Lu, Z., Chen, Y., Sulman, E.P., Xie, K., Böglar, O., et al. (2017). m(6)A Demethylase ALKBH5 Maintains Tumorigenicity of Glioblastoma Stem-like Cells by Sustaining FOXM1 Expression and Cell Proliferation Program. *Cancer Cell* 31, 591–606.e6. <https://doi.org/10.1016/j.ccr.2017.02.013>.
10. Dong, F., Qin, X., Wang, B., Li, Q., Hu, J., Cheng, X., Guo, D., Cheng, F., Fang, C., Tan, Y., et al. (2021). ALKBH5 Facilitates Hypoxia-Induced Par-speckle Assembly and IL8 Secretion to Generate an Immunosuppressive Tumor Microenvironment. *Cancer Res.* 81, 5876–5888. <https://doi.org/10.1158/0008-5472.CAN-21-1456>.
11. Pan, D. (2010). The hippo signaling pathway in development and cancer. *Dev. Cell* 19, 491–505. <https://doi.org/10.1016/j.devcel.2010.09.011>.
12. Zhao, B., Li, L., Lei, Q., and Guan, K.L. (2010). The Hippo-YAP pathway in organ size control and tumorigenesis: an updated version. *Genes Dev.* 24, 862–874. <https://doi.org/10.1101/gad.1909210>.
13. Yu, F.X., and Guan, K.L. (2013). The Hippo pathway: regulators and regulations. *Genes Dev.* 27, 355–371. <https://doi.org/10.1101/gad.210773.112>.
14. Halder, G., and Camargo, F.D. (2013). The hippo tumor suppressor network: from organ size control to stem cells and cancer. *Cancer Res.* 73, 6389–6392. <https://doi.org/10.1158/0008-5472.CAN-13-2392>.
15. Wu, Z., and Guan, K.L. (2021). Hippo Signaling in Embryogenesis and Development. *Trends Biochem. Sci.* 46, 51–63. <https://doi.org/10.1016/j.tibs.2020.08.008>.
16. Bossuyt, W., Chen, C.L., Chen, Q., Sudol, M., McNeill, H., Pan, D., Kopp, A., and Halder, G. (2014). An evolutionary shift in the regulation of the Hippo pathway between mice and flies. *Oncogene* 33, 1218–1228. <https://doi.org/10.1038/onc.2013.82>.
17. Wu, S., Huang, J., Dong, J., and Pan, D. (2003). Hippo encodes a Ste-20 family protein kinase that restricts cell proliferation and promotes apoptosis in conjunction with salvador and warts. *Cell* 114, 445–456. [https://doi.org/10.1016/s0092-8674\(03\)00549-x](https://doi.org/10.1016/s0092-8674(03)00549-x).
18. Jia, J., Zhang, W., Wang, B., Trinko, R., and Jiang, J. (2003). The Drosophila Ste20 family kinase dmST functions as a tumor suppressor by restricting cell proliferation and promoting apoptosis. *Genes Dev.* 17, 2514–2519. <https://doi.org/10.1101/gad.113403>.
19. Harvey, K.F., Pfleger, C.M., and Hariharan, I.K. (2003). The Drosophila Mst ortholog, hippo, restricts growth and cell proliferation and promotes apoptosis. *Cell* 114, 457–467. [https://doi.org/10.1016/s0092-8674\(03\)00557-9](https://doi.org/10.1016/s0092-8674(03)00557-9).

(E) Correlation between mRNA expression levels of LATS2 and ALKBH5 (left) and LATS1 and ALKBH5 (right). Pearson correlation tests were performed using the CGGA datasets.

(F) The correlation analysis between LATS2 and ALKBH5S361ph levels according to IHC analysis in human GBM specimens. Significance was determined by the Pearson correlation test.

(G) A proposed model for the LATS2-ALKBH5 loop. In LATS2-high cells, ALKBH5 is phosphorylated by LATS2, which hinders its nuclear export through CRM1 export and cytoplasmic degradation. The intranuclearly retained ALKBH5, in turn, stabilizes LATS2 mRNA by demethylating m⁶A, thus forming a positive feedback loop. Conversely, in LATS2-low or -negative cells, a subset of ALKBH5 is recognized by CRM1, exported to the cytoplasm, and subjected to ubiquitination and degradation.

20. Udan, R.S., Kango-Singh, M., Nolo, R., Tao, C., and Halder, G. (2003). Hippo promotes proliferation arrest and apoptosis in the Salvador/Warts pathway. *Nat. Cell Biol.* 5, 914–920. <https://doi.org/10.1038/ncb1050>.
21. Pantalacci, S., Tapon, N., and Léopold, P. (2003). The Salvador partner Hippo promotes apoptosis and cell-cycle exit in Drosophila. *Nat. Cell Biol.* 5, 921–927. <https://doi.org/10.1038/ncb1051>.
22. Lai, Z.C., Wei, X., Shimizu, T., Ramos, E., Rohrbaugh, M., Nikolaidis, N., Ho, L.L., and Li, Y. (2005). Control of cell proliferation and apoptosis by mob as tumor suppressor, mats. *Cell* 120, 675–685. <https://doi.org/10.1016/j.cell.2004.12.036>.
23. Huang, J., Wu, S., Barrera, J., Matthews, K., and Pan, D. (2005). The Hippo signaling pathway coordinately regulates cell proliferation and apoptosis by inactivating Yorkie, the Drosophila Homolog of YAP. *Cell* 122, 421–434. <https://doi.org/10.1016/j.cell.2005.06.007>.
24. Dong, J., Feldmann, G., Huang, J., Wu, S., Zhang, N., Comerford, S.A., Gayyed, M.F., Anders, R.A., Maitra, A., and Pan, D. (2007). Elucidation of a universal size-control mechanism in Drosophila and mammals. *Cell* 130, 1120–1133. <https://doi.org/10.1016/j.cell.2007.07.019>.
25. Zhao, B., Wei, X., Li, W., Udan, R.S., Yang, Q., Kim, J., Xie, J., Ikenoue, T., Yu, J., Li, L., et al. (2007). Inactivation of YAP oncprotein by the Hippo pathway is involved in cell contact inhibition and tissue growth control. *Genes Dev.* 21, 2747–2761. <https://doi.org/10.1101/gad.1602907>.
26. Zhou, D., Conrad, C., Xia, F., Park, J.S., Payer, B., Yin, Y., Lauwers, G.Y., Thasler, W., Lee, J.T., Avruch, J., and Bardeesy, N. (2009). Mst1 and Mst2 maintain hepatocyte quiescence and suppress hepatocellular carcinoma development through inactivation of the Yap1 oncogene. *Cancer Cell* 16, 425–438. <https://doi.org/10.1016/j.ccr.2009.09.026>.
27. Camargo, F.D., Gokhale, S., Johnnidis, J.B., Fu, D., Bell, G.W., Jaenisch, R., and Brummelkamp, T.R. (2007). YAP1 increases organ size and expands undifferentiated progenitor cells. *Curr. Biol.* 17, 2054–2060. <https://doi.org/10.1016/j.cub.2007.10.039>.
28. Takahashi, Y., Miyoshi, Y., Takahata, C., Irahara, N., Taguchi, T., Tamaki, Y., and Noguchi, S. (2005). Down-regulation of LATS1 and LATS2 mRNA expression by promoter hypermethylation and its association with biologically aggressive phenotype in human breast cancers. *Clin. Cancer Res.* 11, 1380–1385. <https://doi.org/10.1158/1078-0432.CCR-04-1773>.
29. Peng, Q.S., Cheng, Y.N., Zhang, W.B., Fan, H., Mao, Q.H., and Xu, P. (2020). circRNA_0000140 suppresses oral squamous cell carcinoma growth and metastasis by targeting miR-31 to inhibit Hippo signaling pathway. *Cell Death Dis.* 11, 112. <https://doi.org/10.1038/s41419-020-2273-y>.
30. Ma, B., Chen, Y., Chen, L., Cheng, H., Mu, C., Li, J., Gao, R., Zhou, C., Cao, L., Liu, J., et al. (2015). Hypoxia regulates Hippo signalling through the SIAH2 ubiquitin E3 ligase. *Nat. Cell Biol.* 17, 95–103. <https://doi.org/10.1038/ncb3073>.
31. Gao, Y., Yi, J., Zhang, K., Bai, F., Feng, B., Wang, R., Chu, X., Chen, L., and Song, H. (2017). Downregulation of MiR-31 stimulates expression of LATS2 via the hippo pathway and promotes epithelial-mesenchymal transition in esophageal squamous cell carcinoma. *J. Exp. Clin. Cancer Res.* 36, 161. <https://doi.org/10.1186/s13046-017-0622-1>.
32. Li, Q., Sun, Y., Jarugumilli, G.K., Liu, S., Dang, K., Cotton, J.L., Xiol, J., Chan, P.Y., DeRan, M., Ma, L., et al. (2020). Lats1/2 Sustain Intestinal Stem Cells and Wnt Activation through TEAD-Dependent and Independent Transcription. *Cell Stem Cell* 26, 675–692.e8. <https://doi.org/10.1016/j.stem.2020.03.002>.
33. Cheung, P., Xiol, J., Dill, M.T., Yuan, W.C., Panero, R., Roper, J., Osorio, F.G., Maglic, D., Li, Q., Gurung, B., et al. (2020). Regenerative Reprogramming of the Intestinal Stem Cell State via Hippo Signaling Suppresses Metastatic Colorectal Cancer. *Cell Stem Cell* 27, 590–604.e9. <https://doi.org/10.1016/j.stem.2020.07.003>.
34. Ma, S., Wu, Z., Yang, F., Zhang, J., Johnson, R.L., Rosenfeld, M.G., and Guan, K.L. (2021). Hippo signalling maintains ER expression and ER(+) breast cancer growth. *Nature* 591, E1–E10. <https://doi.org/10.1038/s41586-020-03131-5>.
35. Wen, P.Y., and Kesari, S. (2008). Malignant gliomas in adults. *N. Engl. J. Med.* 359, 492–507. <https://doi.org/10.1056/NEJMra0708126>.
36. Gu, Y., Wang, Y., Wang, Y., Luo, J., Wang, X., Ma, M., Hua, W., Liu, Y., and Yu, F.X. (2020). Hypermethylation of LATS2 Promoter and Its Prognostic Value in IDH-Mutated Low-Grade Gliomas. *Front. Cell Dev. Biol.* 8, 586581. <https://doi.org/10.3389/fcell.2020.586581>.
37. Eyler, C.E., Wu, Q., Yan, K., MacSwords, J.M., Chandler-Mililletto, D., Misuraca, K.L., Lathia, J.D., Forrester, M.T., Lee, J., Stamler, J.S., et al. (2011). Glioma stem cell proliferation and tumor growth are promoted by nitric oxide synthase-2. *Cell* 146, 53–66. <https://doi.org/10.1016/j.cell.2011.06.006>.
38. Li, Z., Bao, S., Wu, Q., Wang, H., Eyler, C., Sathornsumetee, S., Shi, Q., Cao, Y., Lathia, J., McLendon, R.E., et al. (2009). Hypoxia-inducible factors regulate tumorigenic capacity of glioma stem cells. *Cancer Cell* 15, 501–513. <https://doi.org/10.1016/j.ccr.2009.03.018>.
39. Singh, S.K., Hawkins, C., Clarke, I.D., Squire, J.A., Bayani, J., Hide, T., Henkelman, R.M., Cusimano, M.D., and Dirks, P.B. (2004). Identification of human brain tumour initiating cells. *Nature* 432, 396–401. <https://doi.org/10.1038/nature03128>.
40. Lathia, J.D., Mack, S.C., Mulkearns-Hubert, E.E., Valentim, C.L.L., and Rich, J.N. (2015). Cancer stem cells in glioblastoma. *Genes Dev.* 29, 1203–1217. <https://doi.org/10.1101/gad.261982.115>.
41. Li, Y., Wang, W., Wang, F., Wu, Q., Li, W., Zhong, X., Tian, K., Zeng, T., Gao, L., Liu, Y., et al. (2017). Paired related homeobox 1 transactivates dopamine D2 receptor to maintain propagation and tumorigenicity of glioma-initiating cells. *J. Mol. Cell Biol.* 9, 302–314. <https://doi.org/10.1093/jmcb/mjx017>.
42. Dong, F., Li, Q., Yang, C., Huo, D., Wang, X., Ai, C., Kong, Y., Sun, X., Wang, W., Zhou, Y., et al. (2018). PRMT2 links histone H3R8 asymmetric dimethylation to oncogenic activation and tumorigenesis of glioblastoma. *Nat. Commun.* 9, 4552. <https://doi.org/10.1038/s41467-018-06968-7>.
43. Visvanathan, A., Patil, V., Arora, A., Hegde, A.S., Arivazhagan, A., Santosh, V., and Somasundaram, K. (2018). Essential role of METTL3-mediated m(6)A modification in glioma stem-like cells maintenance and radioresistance. *Oncogene* 37, 522–533. <https://doi.org/10.1038/onc.2017.351>.
44. Li, F., Yi, Y., Miao, Y., Long, W., Long, T., Chen, S., Cheng, W., Zou, C., Zheng, Y., Wu, X., et al. (2019). N(6)-Methyladenosine Modulates Nonsense-Mediated mRNA Decay in Human Glioblastoma. *Cancer Res.* 79, 5785–5798. <https://doi.org/10.1158/0008-5472.CAN-18-2868>.
45. Zhang, Y., Geng, X., Li, Q., Xu, J., Tan, Y., Xiao, M., Song, J., Liu, F., Fang, C., and Wang, H. (2020). m6A modification in RNA: biogenesis, functions and roles in gliomas. *J. Exp. Clin. Cancer Res.* 39, 192. <https://doi.org/10.1186/s13046-020-01706-8>.
46. Okada, T., Lopez-Lago, M., and Giancotti, F.G. (2005). Merlin/NF-2 mediates contact inhibition of growth by suppressing recruitment of Rac to the plasma membrane. *J. Cell Biol.* 171, 361–371. <https://doi.org/10.1083/jcb.200503165>.
47. Kim, N.G., Koh, E., Chen, X., and Gumbiner, B.M. (2011). E-cadherin mediates contact inhibition of proliferation through Hippo signaling-pathway components. *Proc. Natl. Acad. Sci. USA* 108, 11930–11935. <https://doi.org/10.1073/pnas.1103345108>.
48. Yu, F.X., Zhao, B., Panupinthu, N., Jewell, J.L., Lian, I., Wang, L.H., Zhao, J., Yuan, H., Tumaneng, K., Li, H., et al. (2012). Regulation of the Hippo-YAP pathway by G-protein-coupled receptor signaling. *Cell* 150, 780–791. <https://doi.org/10.1016/j.cell.2012.06.037>.
49. Nakai, K., and Horton, P. (1999). PSORT: a program for detecting sorting signals in proteins and predicting their subcellular localization. *Trends Biochem. Sci.* 24, 34–36. [https://doi.org/10.1016/s0968-0004\(98\)01336-x](https://doi.org/10.1016/s0968-0004(98)01336-x).
50. Qin, X., Long, Y., Bai, X., Cao, L., Yan, H., Zhang, K., Wang, B., and Wu, X. (2023). The disordered C terminus of ALKBH5 promotes phase separation and paraspeckles assembly. *J. Biol. Chem.* 299, 105071. <https://doi.org/10.1016/j.jbc.2023.105071>.

51. Fornerod, M., Ohno, M., Yoshida, M., and Mattaj, I.W. (1997). CRM1 is an export receptor for leucine-rich nuclear export signals. *Cell* 90, 1051–1060. [https://doi.org/10.1016/s0092-8674\(00\)80371-2](https://doi.org/10.1016/s0092-8674(00)80371-2).
52. Fung, H.Y.J., Fu, S.C., and Chook, Y.M. (2017). Nuclear export receptor CRM1 recognizes diverse conformations in nuclear export signals. *eLife* 6, e23961. <https://doi.org/10.7554/elife.23961>.
53. Furth, N., and Aylon, Y. (2017). The LATS1 and LATS2 tumor suppressors: beyond the Hippo pathway. *Cell Death Differ.* 24, 1488–1501. <https://doi.org/10.1038/cdd.2017.99>.
54. Luo, X., Li, H., Liang, J., Zhao, Q., Xie, Y., Ren, J., and Zuo, Z. (2021). RMVar: an updated database of functional variants involved in RNA modifications. *Nucleic Acids Res.* 49, D1405–D1412. <https://doi.org/10.1093/nar/gkaa811>.
55. Seo, G., Han, H., Vargas, R.E., Yang, B., Li, X., and Wang, W. (2020). MAP4K Interactome Reveals STRN4 as a Key STRIPAK Complex Component in Hippo Pathway Regulation. *Cell Rep.* 32, 107860. <https://doi.org/10.1016/j.celrep.2020.107860>.
56. Moroishi, T., Park, H.W., Qin, B., Chen, Q., Meng, Z., Plouffe, S.W., Taniguchi, K., Yu, F.X., Karin, M., Pan, D., and Guan, K.L. (2015). A YAP/TAZ-induced feedback mechanism regulates Hippo pathway homeostasis. *Genes Dev.* 29, 1271–1284. <https://doi.org/10.1101/gad.262816.115>.
57. Zhao, B.S., Roundtree, I.A., and He, C. (2017). Post-transcriptional gene regulation by mRNA modifications. *Nat. Rev. Mol. Cell Biol.* 18, 31–42. <https://doi.org/10.1038/nrm.2016.132>.
58. Slobodin, B., Bahat, A., Sehrawat, U., Becker-Herman, S., Zuckerman, B., Weiss, A.N., Han, R., Elkon, R., Agami, R., Ulitsky, I., et al. (2020). Transcription Dynamics Regulate Poly(A) Tails and Expression of the RNA Degradation Machinery to Balance mRNA Levels. *Mol. Cell* 78, 434–444.e5. <https://doi.org/10.1016/j.molcel.2020.03.022>.
59. Hou, G., Zhao, X., Li, L., Yang, Q., Liu, X., Huang, C., Lu, R., Chen, R., Wang, Y., Jiang, B., and Yu, J. (2021). SUMOylation of YTHDF2 promotes mRNA degradation and cancer progression by increasing its binding affinity with m6A-modified mRNAs. *Nucleic Acids Res.* 49, 2859–2877. <https://doi.org/10.1093/nar/gkab065>.
60. Yu, F., Wei, J., Cui, X., Yu, C., Ni, W., Bungert, J., Wu, L., He, C., and Qian, Z. (2021). Post-translational modification of RNA m6A demethylase ALKBH5 regulates ROS-induced DNA damage response. *Nucleic Acids Res.* 49, 5779–5797. <https://doi.org/10.1093/nar/gkab415>.
61. Raj, N., Wang, M., Seoane, J.A., Zhao, R.L., Kaiser, A.M., Moonie, N.A., Demeter, J., Boutelle, A.M., Kerr, C.H., Mulligan, A.S., et al. (2022). The Mettl3 epitranscriptomic writer amplifies p53 stress responses. *Mol. Cell* 82, 2370–2384.e10. <https://doi.org/10.1016/j.molcel.2022.04.010>.
62. Zhang, C., Samanta, D., Lu, H., Bullen, J.W., Zhang, H., Chen, I., He, X., and Semenza, G.L. (2016). Hypoxia induces the breast cancer stem cell phenotype by HIF-dependent and ALKBH5-mediated m(6)A-demethylation of NANOG mRNA. *Proc. Natl. Acad. Sci. USA* 113, E2047–E2056. <https://doi.org/10.1073/pnas.1602883113>.
63. Lan, Q., Liu, P.Y., Bell, J.L., Wang, J.Y., Hüttelmaier, S., Zhang, X.D., Zhang, L., and Liu, T. (2021). The Emerging Roles of RNA m(6)A Methylation and Demethylation as Critical Regulators of Tumorigenesis, Drug Sensitivity, and Resistance. *Cancer Res.* 81, 3431–3440. <https://doi.org/10.1158/0008-5472.CAN-20-4107>.
64. Qiu, X., Yang, S., Wang, S., Wu, J., Zheng, B., Wang, K., Shen, S., Jeong, S., Li, Z., Zhu, Y., et al. (2021). M(6)A Demethylase ALKBH5 Regulates PD-L1 Expression and Tumor Immunoenvironment in Intrahepatic Cholangiocarcinoma. *Cancer Res.* 81, 4778–4793. <https://doi.org/10.1158/0008-5472.CAN-21-0468>.
65. Shen, C., Sheng, Y., Zhu, A.C., Robinson, S., Jiang, X., Dong, L., Chen, H., Su, R., Yin, Z., Li, W., et al. (2020). RNA Demethylase ALKBH5 Selectively Promotes Tumorigenesis and Cancer Stem Cell Self-Renewal in Acute Myeloid Leukemia. *Cell Stem Cell* 27, 64–80.e9. <https://doi.org/10.1016/j.stem.2020.04.009>.
66. Lv, D., Zhong, C., Dixit, D., Yang, K., Wu, Q., Godugu, B., Prager, B.C., Zhao, G., Wang, X., Xie, Q., et al. (2023). EGFR promotes ALKBH5 nuclear retention to attenuate N6-methyladenosine and protect against ferroptosis in glioblastoma. *Mol. Cell* 83, 4334–4351.e7. <https://doi.org/10.1016/j.molcel.2023.10.025>.
67. Fang, L., Teng, H., Wang, Y., Liao, G., Weng, L., Li, Y., Wang, X., Jin, J., Jiao, C., Chen, L., et al. (2018). SET1A-Mediated Mono-Methylation at K342 Regulates YAP Activation by Blocking Its Nuclear Export and Promotes Tumorigenesis. *Cancer Cell* 34, 103–118.e9. <https://doi.org/10.1016/j.ccr.2018.06.002>.
68. Ran, F.A., Hsu, P.D., Wright, J., Agarwala, V., Scott, D.A., and Zhang, F. (2013). Genome engineering using the CRISPR-Cas9 system. *Nat. Protoc.* 8, 2281–2308. <https://doi.org/10.1038/nprot.2013.143>.
69. Dai, Z., Li, R., Hou, Y., Li, Q., Zhao, K., Li, T., Li, M.J., and Wu, X. (2021). Inducible CRISPRa screen identifies putative enhancers. *J Genet Genomics* 48, 917–927. <https://doi.org/10.1016/j.jgg.2021.06.012>.
70. Xiang, Y., Laurent, B., Hsu, C.H., Nachtergaelie, S., Lu, Z., Sheng, W., Xu, C., Chen, H., Ouyang, J., Wang, S., et al. (2017). RNA m6A methylation regulates the ultraviolet-induced DNA damage response. *Nature* 543, 573–576. <https://doi.org/10.1038/nature21671>.
71. Li, Q., Lv, X., Han, C., Kong, Y., Dai, Z., Huo, D., Li, T., Li, D., Li, W., Wang, X., et al. (2022). Enhancer reprogramming promotes the activation of cancer-associated fibroblasts and breast cancer metastasis. *Theranostics* 12, 7491–7508. <https://doi.org/10.7150/thno.75853>.
72. Huo, D., Yu, Z., Li, R., Gong, M., Sidoli, S., Lu, X., Hou, Y., Dai, Z., Kong, Y., Liu, G., et al. (2022). CpG island reconfiguration for the establishment and synchronization of polycomb functions upon exit from naive pluripotency. *Mol. Cell* 82, 1169–1185.e7. <https://doi.org/10.1016/j.molcel.2022.01.027>.

STAR★METHODS

KEY RESOURCES TABLE

REAGENT or RESOURCE	SOURCE	IDENTIFIER
Antibodies		
ALKBH5	Sigma	Cat# HPA007196; RRID:AB_1850461
β-ACTIN	Abclonal	Cat# AC026; RRID: AB_2768234
GAPDH	Abclonal	Cat# AC002; RRID: AB_2736879
METTL3	Proteintech	Cat# 15073-1-AP; RRID: AB_2142033
METTL14	Proteintech	Cat# 26158-1-AP; RRID: AB_2800447
FTO	Proteintech	Cat# 27226-1-AP; RRID: AB_2880809
WTAP	Proteintech	Cat# 60188-1-Ig; RRID: AB_10859484
YTHDF1	Proteintech	Cat# 17479-1-AP; RRID: AB_2217473
LATS2	Abcam	Cat# ab135794; RRID: AB_3095796
SOX2	CST	Cat# 4900S; RRID: AB_10560516
FLAG	CWBIO	Cat# CW0287M; RRID: AB_3095798
GFP	Absin	Cat# abs158384; RRID: AB_3095802
Myc	Proteintech	Cat# 60003-2-Ig; RRID: AB_2734122
m ⁶ A	Milipore	Cat# ABE572; RRID: AB_3095804
LATS1	Proteintech	Cat# 17049-1-AP; RRID: AB_2281011
pLATS1/2	Abclonal	Cat# AP0904; RRID: AB_2771258
YAP	Cell Signaling Technology	Cat #12395; RRID: AB_2797897
pYAP	Absin	Cat# abs106569; RRID: AB_3095803
Bacterial and virus strains		
DH5α competent cell	TIANGEN	Cat# CB101-02
Biological samples		
DNA samples extracted from GL261 cell	This paper	N/A
RNA samples extracted from GL261 cell	This paper	N/A
Chemicals, peptides, and recombinant proteins		
TRULI	Selleck	Cat #E1061
bFGF	Sino Biological	Cat #10014-HNAE
EGF	Sino Biological	Cat #10605-HNAE
Deposited data		
RNA-seq	This paper	GSE161863
MeRIP-seq	This paper	GSE255348
Mass spectrometry proteomics data	Qin et al. ⁵⁰	PXD042183
Experimental models: Cell lines		
NIH3T3	ATCC	Cat #XY-XB-1626
HCT116	ATCC	Cat #CCL-247
HEK 293T	ATCC	Cat #CRL-3216
GL261	This paper	N/A
TPC1115	This paper	N/A
Experimental models: Organisms/strains		
Mouse: C57BL/6J	The Jackson Laboratory	Strain #:000664 RRID:IMSR_JAX:000664
Mouse: Balb/C nude	Charles River Japan (CRJ)	Strain Code 194
Oligonucleotides		
See Table S2 for details	This paper	N/A

(Continued on next page)

Continued

REAGENT or RESOURCE	SOURCE	IDENTIFIER
Software and algorithms		
Prism v9	GraphPad Software	https://www.graphpad.com/scientific-software/prism/
FIJI	ImageJ	https://imagej.net/software/fiji/
FlowJo	BD and Company	https://www.flowjo.com/solutions/flowjo
Other		
DMEM/F12	Thermo Fisher Scientific	Cat# 11320033
DMEM	Thermo Fisher Scientific	Cat# 12491015
RPMI 1640	Thermo Fisher Scientific	Cat #21870-076
Fetal Bovine Serum	GeminiBio	Cat#100-106, Lot #A33H00L
Penicillin and Streptomycin	Gibco	Cat # 15070063
N2	Gibco	Cat # 17502048
B27	Gibco	Cat # 17504044
X-tremeGENE HP DNA Transfection Reagent		N/A
Anti-FLAG M2 Magnetic Beads	Sigma-Aldrich	Cat# M8823
Complete protease inhibitor cocktail tablets	Sigma-Aldrich	Cat# 05056489001
DAPI	Cell Signaling Technology	Cat# 4083
Amersham Hybond-N + membrane	Cytiva	RPN303B
Dual-Glo® Luciferase Assay System	Promega	Cat#E2920
TRIzol	Invitrogen	Cat#15596026
VAHTS Total RNA-seq (H/M/R) Library Prep Kit	Vazyme	Cat##NR603

RESOURCE AVAILABILITY

Lead contact

Further information and requests for resources and reagents should be directed to and will be fulfilled by the lead contact, Xudong Wu (wuxudong@tmu.edu.cn).

Materials availability

The plasmids and cell lines generated in this study are available on request to the [lead contact](#).

Data and code availability

- The primary data supporting the results in this study are available within the paper and its supplemental information. The raw sequence data of RNA-seq and MeRIP-seq in this study have been deposited in the NCBI Gene Expression Omnibus under accession GSE161863 and GSE255348. The mass spectrometry proteomics data have been deposited to the ProteomeXchange Consortium via the PRIDE partner repository with the dataset identifier PXD042183.
- This paper does not report original code.
- Any additional information required to reanalyze the data reported in this paper is available from the [lead contact](#) upon request.

EXPERIMENTAL MODEL AND STUDY PARTICIPANT DETAILS

Cell culture

Cell lines including GL261, HEK293T, HCT116, NIH3T3 were cultured in DMEM containing 10% FBS. The primary TPC1115 cells were obtained from fresh surgical specimens of human primary GBMs and cultured as either monolayer or tumor spheres in DMEM/F12 medium supplemented with N2, B27 (Gibco), 20 ng/mL human fibroblast growth factor-basic (bFGF, Sino Biological, Beijing, China), 10 ng/mL epidermal growth factor-basic (EGF, Sino Biological, Beijing, China). To observe the effects of serum deprivation, TPC1115 cells were transiently cultured in DMEM containing 10% FBS as a control. All cells were maintained at 37°C in a humid incubator with 5% CO₂. To generate xenograft models, cells were lentivirally transduced to express luciferase. All cells were maintained at 37°C with 5% CO₂ and regularly tested for Mycoplasma free.

Animal model

The animal study protocol was approved by the Institutional Animal Use and Care Committee at Tianjin Medical University. This study was approved by The Research Ethics Committee of Tianjin Medical University (TMUaMEC-2017009). All mice used for

in vivo experiments were female at the age of 4–6 weeks old and purchased from Beijing Huafukang Bioscience Co., Inc. (Beijing, China).

Human tumor samples and ethics approval

The collection and usage of patient tumor tissue samples were approved by the Research Ethics Committee of Tongji Hospital, Tongji Medical College, Huazhong University of Science and Technology (serial no.TJ-IBR20181111).

METHOD DETAILS

Plasmid construction

ALKBH5 expression plasmid was generated by cloning the full-length open reading frame of human ALKBH5 gene (NM_017758.3) into pCDH-CMV-MCS-EF1-Puro (SBI) and pGEX6p-1 with a fusion of 3×FLAG at the N-terminal. ALKBH5 S361A and ALKBH5 S361D constructs were generated by site-directed mutagenesis (Transgene). pCDNA-Myc LATS2, pCDNA-Myc LATS2 K697A, pLKO.1-shLATS2-1, pLKO.1-shLATS2-2 and expression plasmids for GFP-tagged CRM1 were used in previous studies.^{30,67} Specific guide RNA for mouse Lats2 was designed and cloned into the PX459 vector.⁶⁸ Specific guide RNAs for human LATS1, MST1 and MST2 were designed and cloned into the plentiCRISPR V2 vector. Specific oligonucleotides against human ALKBH5 were designed and cloned into pLKO.1 vector according to the recommended Addgene protocol. LATS2 3'UTR was PCR amplified and cloned into pLS0 vector. Site-directed mutagenesis was taken to construct mutants. All primers and oligonucleotide sequences used in this study are listed in Table S1.

Co-IP, western blot, and luciferase reporter assays

X-tremeGENE HP DNA Transfection Reagent was used for transiently transfection according to instruction. Transfected cells were harvested and lysed in 2×loading buffer (0.25 M Tris-HCl pH 6.8, DTT 78 mg/mL, SDS 100 mg/mL, 50% Glycerine, 5 mg/mL bromophenol blue) after 36 h (hrs) for WB analysis. For Co-immunoprecipitation (Co-IP), cells were lysed in NP-40 buffer (150 mM NaCl, 1% Triton X-100, 10 mM Tris pH 7.4, 1 mM EDTA pH 8.0, 1 mM EGTA pH 8.0, 0.5% NP-40, 1 mM PMSF) for 30 min (min) at 4°C. The supernatants of the samples after centrifugation were incubated with antibodies for 2–4 h at 4°C. Then 20 µL Protein A/G agarose (GE, 10080881) were added for another 2 h incubation at 4°C. Beads were washed three times with NP-40 buffer, followed by WB assay. Relevant antibodies are listed in Table S2. Polyclonal antibodies of ALKBH5S361ph were generated with specific phosphorylated peptides by Abclonal. Luciferase reporter assay was performed by utilizing Dual-Glo Luciferase Assay System.⁶⁹

Dot blot

The m6A dot blot assay was performed based on a modified protocol.⁷⁰ Following the manufacturer's instruction, total RNA was extracted by TRIzol method. Then, the extracted RNAs were gradient diluted, loaded and UV crosslinked onto Amersham Hybond-N + membrane (GE Healthcare, Chicago, IL). The membrane was then blocked with 5% nonfat milk in 1×PBST for 1 h and then incubated with an anti-m6A antibody overnight at 4°C, and then subjected to horseradish peroxidase (HRP)-conjugated secondary antibody and visualization by an ECL Detection Kit. Methylene blue staining was performed to compare RNA loading.

Intracranial Xenotransplantation

For intracranial injection, 2×10⁵ of TPC1115-luc cells or GL261-luc cells were transplanted into the frontal lobes of brains of Balb/C nude mice or C57BL/6J mice respectively. Tumor growth was visualized by bioluminescence xenogen imaging and the survival was recorded and analyzed accordingly.⁴²

IHC and IF

Immunohistochemistry (IHC) and Immunofluorescence (IF) analyses were modified from a previous protocol.⁷¹ Briefly, tissue slides from tumor xenografts or surgical specimens were de-paraffinized, rehydrated through an alcohol series followed by antigen retrieval with sodium citrate buffer. Tumor sections were blocked with 5% BSA containing with 0.1% Triton X-100 in PBS for 20 min at room temperature and then incubated overnight with primary antibodies 4°C overnight. IHC staining was performed with HRP conjugates using DAB detection. IF staining was performed with appropriate FITC or TRITC-secondary antibody (ZSBIO, dilution 1:200) and mounted with Fluoromount-G medium (Southern Biotech, 0100-01). For IF analysis of cultured cells, cells were fixed with 4% formaldehyde (Fisher) for 15 min and then blocked with 5% BSA with 0.1% Triton X-100 in PBS for 20 min at room temperature. Immunostaining was performed using the appropriate primary and secondary antibodies.

RT-qPCR and MeRIP-qPCR analysis

For RT-qPCR analysis, total RNA was isolated from samples with TRIzol reagents (Ambion) following the manufacturer's instructions. cDNA was prepared with the Superscript Reverse Transcriptase (Invitrogen). Quantitative PCR was performed using SYBR Green Master Mix (Thermo). MeRIP-qPCR was performed as previously described.¹⁰ Briefly, 5 µg of total RNA was adjusted to 18 µL with RNase-free water. Then 2 µL of 10×RNA fragmentation buffer (100 mmol/L Tris-HCl, 100 mmol/L ZnCl₂) in nuclease-free

H_2O) was added and incubated in a preheated thermal cycler for approximately 5 min at 70°C. 2 μL of 0.5 mol/L EDTA was added to stop the reaction. The total RNA was chemically fragmented into approximately 200-nt-long fragments. 30 μL of protein G magnetic beads were tumbled with 5 μg anti-m⁶A antibody (Millipore, ABE572) at 4°C overnight. The antibody-bead mixture was resuspended in 500 μL of the IP reaction mixture with fragmented total RNA, 100 μL of 5× IP buffer, and 5 μL of RNase Inhibitor and incubated for 2 h at 4°C. After being washed by the low/high salt-washing buffer, the m6A-enriched RNA was eluted with 14 μL ultrapure H_2O according to the instructions of RNeasy Mini Kit (QIAGEN). Primers used for qPCR analyses in this study are listed in Table S2.

RNA-seq, MeRIP-seq and data analysis

Total RNA was isolated from *Lats2* KO and control GL261 cells using Trizol reagent (Takara). Poly(A) RNA from 1 μg total RNA was used to generate the cDNA library according to Truseq RNA Sample Prep Kit protocol, which was then sequenced using an BGISEQ platform. For RNA-sequencing (RNA-seq) analysis, clean reads were aligned to the reference genome with Hisat2 with default parameters, and the aligned reads were used to quantify mRNA expression by using featureCounts. DESeq2 was employed for data normalization and differential expression analysis of RNA-seq counts.⁷² For MeRIP-seq, more than 250 μg of total RNA was extracted from each group. The mRNA was further enriched using oligo (dT) beads and then chemically fragmented into ~ 200 nt nucleotides with fragmentation buffer. The m6A-modified mRNA was immunoprecipitated with anti-m⁶A antibodies and eluted for RNA sequencing. Libraries for input mRNA (RNA-seq) and m⁶A-enriched mRNA were simultaneously constructed with the VAHTS Total RNA-seq (H/M/R) Library Prep Kit for Illumina (Vazyme#NR603), followed by sequencing with the PE150 strategy. The raw data were aligned to human genome GRCh37/hg19 by the HISAT2 software (v2.0.5). Then m⁶A peaks were determined by the ExomePeak software (v2.6.0) and annotated according to the Ensembl database. Integrative Genomics Viewer (IGV) software was applied to present the visualization of the m⁶A peaks.

QUANTIFICATION AND STATISTICAL ANALYSIS

All grouped data are presented as mean \pm SD. Unpaired Student's *t*-tests are presented as mean \pm SD during comparison between unpaired two-groups and one-way ANOVA was applied for multi-group data comparison. The variance was similar between the groups that were statistically compared. Pearson correlation test was used as appropriate. Kaplan-Meier curves were generated and log rank analysis was performed using GraphPad Software. Significant differences for all quantitative data were considered when **p* < 0.05, ***p* < 0.01. Precise *p*-values are explicitly indicated for *p* < 0.01.